

JGR Atmospheres

RESEARCH ARTICLE

10.1029/2019JD030693

Key Points:

- A novel physics-based yet computationally efficient model of the lightning channel nonlinear resistance is introduced
- The model reproduces the finite time scale of streamer-to-leader transition and the steady-state negative differential resistance
- The model captures the experimentally inferred direct relationship between electrical and optical properties of rocket-triggered lightning

Correspondence to:

C. L. da Silva, caitano.dasilva@nmt.edu

Citation:

da Silva, C. L., Sonnenfeld, R. G., Edens, H. E., Krehbiel, P. R., Quick, M. G., & Koshak, W. J. (2019). The plasma nature of lightning channels and the resulting nonlinear resistance. *Journal of Geophysical Research: Atmospheres*, 124, 9442–9463. https://doi.org/10.1029/2019JD030693

Received 28 MAR 2019 Accepted 30 JUL 2019 Accepted article online 5 AUG 2019 Published online 19 AUG 2019

The Plasma Nature of Lightning Channels and the Resulting Nonlinear Resistance

C. L. da Silva¹, R. G. Sonnenfeld¹, H. E. Edens¹, P. R. Krehbiel¹, M. G. Quick², and W. J. Koshak³

¹Department of Physics and Langmuir Laboratory, New Mexico Institute of Mining and Technology, Socorro, NM, USA, ²Earth System Science Interdisciplinary Center, University of Maryland, College Park, MD, USA, ³NASA Marshall Space Flight Center, Huntsville, AL, USA

Abstract Lightning channels are made of plasma. As a consequence, the driving electrical current changes the channel's resistance in a nonlinear fashion. The resistance has an intricate dependence on the history of Joule heating and various cooling processes, as well as on the various kinetic processes that dictate the population balance of electrons within the channel. Such dependence cannot be captured by an analytic function, as often attempted. In this paper, we introduce a minimal numerical model that can qualitatively capture the temporal dynamics of the key plasma properties of a lightning channel, including its electric field, temperature, plasma density, radius, and the resulting nonlinear resistance. Through a series of novel parameterizations, we introduce six zero-dimensional equations that can capture both nonequilibrium/low-temperature and local thermodynamic equilibrium/high-temperature plasma regimes. In this manuscript, we go to great lengths to validate the model, showing that it can reproduce the finite time scale of streamer-to-leader transition, replicate the negative differential resistance behavior of steady-state plasma arcs, and properly describe the temporal evolution of temperature in a return stroke channel. Finally, the model is applied to the simulation of optical emissions from rocket-triggered lightning strikes, explaining the measured delay between the rise of current and visible light, as well as reproducing the direct relationship between peak current and peak radiated power and between charge transferred to ground and total radiated energy.

Plain Language Summary A number of unsolved puzzles in lightning physics are rooted in the plasma nature of lightning channels. One such example is why do negative cloud-to-ground lightning flashes transfer charge to ground in a series of multiple strikes that reuse the same channel, while positive flashes mostly have a single stroke? In this paper we introduce a computer simulation tool to capture the plasma nature of lightning and model its properties. One of the key results presented here is the model's ability to explain the experimentally derived relationship between optical and electrical properties in triggered lightning flashes.

1. Introduction

Lightning channels are filaments of ionized air that exhibit collective behavior, or in other words, they are atmospheric *plasmas*. The basic elements of a lightning flash are streamers, leaders, and the return stroke channel (Bazelyan & Raizer, 2000, Chapters 2 and 4). Streamers are nonlinear plasma ionization waves characterized by high-electric fields (enhanced by space charge) and near-ambient temperature (Raizer, 1991, section 12.3). Streamers fan out of the leader tip carving the way for its propagation. Leaders are characterized by high plasma temperature (>5,000 K) and consequently low resistance, resulting in their ability to propagate tens of kilometers in the Earth's atmosphere (Bazelyan & Raizer, 2000, Chapter 2). The return stroke is a neutralization wave that follows the lightning discharge's connection to a ground structure. An intense surge current travels upward completely transforming the channel. Intense energy deposition brings the temperature to $\geq 30,000$ K, achieving near-local thermodynamic equilibrium (LTE). The return stroke creates a pathway for several modes of charge transfer to ground (e.g., M components, dart leaders, and continuing current, see Rakov & Uman, 2003, sections 1.2, 1.3, 4.6–4.10, and 12.2–12.5).

Differently than the return stroke channel, streamers and leaders in lightning are nonequilibrium plasmas, a special category characterized by short lifetimes, electron temperatures much larger than of neutrals, high

©2019. American Geophysical Union. All Rights Reserved.



collision rates between charged and neutral particles, and low degree of ionization (see, e.g., Becker et al., 2004). Streamers, for instance, only partially meet the three standard conditions that traditionally define a plasma (Bittencourt, 2004; pp. 6–11). These criteria define the plasma's ability to shield short-range electrostatic interactions between individual particles, remain quasi-neutral, and respond collectively to long-range electromagnetic forces. The three conditions can be estimated for typical streamer properties at atmospheric pressure, that is, electron temperature of 23,000 K, or \sim 2 eV, and electron density of 10^{18} – 10^{20} m⁻³ (Raizer, 1991; section 12.3). First, the Debye length is \sim 1–10 μ m, which is relatively smaller than the streamer radius, \sim 0.1–1 mm (Naidis, 2009). Second, there are many electrons in a Debye sphere, \sim 500–5,000. Third, the electron-neutral collision frequency is \sim 10^{12} s⁻¹, which is higher than the frequency of relevant processes, including the plasma frequency. Therefore, it can be said that the first two conditions are approximately met, but not the third one. On the other hand, it is easy to show that all three conditions are met in the return stroke channel. Therefore, even though the formal definition of a plasma is not always met within the many elements of a lightning flash, we refer to its constituting ionized gas as a "plasma," because it remains quasi-neutral and responds collectively to applied electric fields.

The aforementioned collective behavior in lightning is evidenced in the many types of ionization waves (e.g., streamer front, leader front, dart leaders, and return strokes), its ability to shield itself from externally applied electric fields, and its negative differential resistance, which in its turn map into several phenomenological features, including its fractal structure, the contrasting behavior of positively and negatively charged extremities, and the fact that leader channels are enveloped by streamer zones and corona sheaths. This manuscript focus on perhaps the most important feature attributed to the plasma nature of lightning—its nonlinear resistance. A correct description of the channel resistance is required to better characterize lightning electromagnetic emissions, to correctly predict its deleterious effects in man-made structures, to quantify the impacts of lightning in atmospheric chemistry, and to address fundamental open questions regarding lightning initiation, propagation, and polarity asymmetries. The nonlinear plasma resistance is in its turn dependent on the history of energy deposition and losses in the channel and cannot be accurately determined without properly tracking the evolution of all other channel properties, including electric field, electron density, temperature, and radius.

Efforts to characterize the nonlinear resistance and overall plasma properties of the lightning channel can be classified into three categories: (1) LTE gas-dynamic models (Aleksandrov et al., 2000; Chemartin et al., 2009; Hill, 1971; Paxton et al., 1986; Plooster, 1971; Ripoll et al., 2014a), (2) streamer-to-leader transition models (Aleksandrov et al., 2001; Bazelyan et al., 2007; da Silva & Pasko, 2013; da Silva, 2015; Gallimberti, 1979; Gallimberti et al., 2002; Popov, 2003; 2009), and (3) semiempirical resistance models (Baker, 1990; De Conti et al., 2008; Koshak et al., 2015; Mattos & Christopoulos, 1990; Theethayi & Cooray, 2005). The three categories are described in the upcoming paragraphs. Instructive discussions and additional references regarding each of the three categories can also be found in sections 2.5, 2.3, and 4.4, respectively, of Bazelyan and Raizer's (2000) textbook. On a separate note, the literature concerning the resistance of short spark discharges in the laboratory is very rich and has provided many insights into building the models cited above (see, e.g., Engel et al., 1989; Kushner et al., 1985; Marode et al., 1979; Naidis, 1999; Riousset et al., 2010; Takaki & Akiyama, 2001). It is outside of our scope to provide a detailed review of these investigations, but it can easily be found elsewhere (da Silva & Pasko, 2013; Engel et al., 1989; Montano et al., 2006).

The first group of investigations evaluates the resistance of a lightning channel under the assumption that the plasma is in LTE. In this framework, the electrical conductivity is only a function of temperature, that is, $\sigma = \sigma(T)$, which is valid for atmospheric-pressure arcs at temperatures higher than ~10,000 K, where T or simply the word "temperature" here and in the remainder of this manuscript corresponds to the temperature of the neutral gas. (The 10,000-K threshold is a rough estimate; see section 2.2 for justifications.) Following the return stroke simulations performed by Plooster (1971), these models describe how Joule heating deposition in the channel core heats the air and causes rapid hydrodynamic expansion. They solve a system of three equations accounting for conservation of mass, momentum, and energy (or enthalpy) of the neutral gas (air). They are often solved in a 1-D radial domain, with the exception being the work of Chemartin et al. (2009) where efforts are made to capture the 3-D tortuosity of a plasma arc. A few of these models also present a detailed description of the plasma radiative transfer (see, e.g., Paxton et al., 1986; Ripoll et al., 2014a).



The second class is dedicated to a detailed description of the streamer-to-leader transition process, which takes place during the discharge onset or at the tip of a growing channel. Streamer-to-leader transition is the name given to the sequence of processes converting cold and low-conductivity plasma channels (streamers) into hot and highly conducting ones (leaders), a condition required to allow lightning channels to propagate for several kilometers in the atmosphere before decaying (Bazelyan & Raizer, 2000, p. 59). These models account for the hydrodynamic expansion of the neutral gas, such as the ones described in the first category. However, following in the footsteps of the seminal monograph by Gallimberti (1979), they also account for a non-LTE plasma conductivity arising from the detailed kinetic balance of an air plasma. The more recent models describe in detail the energy exchange between charged and neutral particles accounting for the partitioning of electronic power between elastic collisions, and excitation of vibrational and electronic states, and also delayed vibrational energy relaxation of nitrogen molecules (see, e.g., da Silva & Pasko, 2013). The non-LTE conductivity regime encompasses temperatures lower than ~10,000 K. The models in this category (cited in this paragraph) do not account for photoionization, which is important at the high temperatures present in the return stroke channel.

The third category groups investigations where a semiempirical expression for the channel resistance (per unit length) as a function of time, R(t), has been employed in return stroke simulations. The reasoning behind such approach is that it is impractical to use the self-consistent gas-dynamic simulations to calculate the resistance of a channel that is 5 (or more) orders of magnitude longer than wider. Therefore, a parametric dependence for R(t) facilitates the implementation of a height-dependent, transmission-line-like return stroke model. These investigations use expressions for R(t) derived by Barannik et al. (1975), Kushner et al. (1985), and others, as reviewed by De Conti et al. (2008). To the best of our knowledge, only Liang et al. (2014) present an effort to couple a self-consistent resistance calculation with a transmission-line-like return stroke model. These authors use a two-temperature plasma model to infer the electronic conductivity. The model does not account for channel expansion or plasma chemistry, and it is unclear how well it compares to the conventional gas-dynamic return stroke simulations. Nonetheless, investigations such as done by De Conti et al. (2008) and Liang et al. (2014) raise the need for accurate and computationally efficient models for R(t).

The objective of this work is to fill a gap in the peer-reviewed literature by introducing a comprehensive—yet simple—model that can exemplify the plasma nature of lightning channels (section 2.1). We describe a series of parameterizations that allow us to capture both the low-temperature/non-LTE and the high-temperature/LTE regimes, account for radial expansion, and include negative-ion chemistry, at little computational cost (section 2.2). The model is first tested by calculating the time scale for streamer-to-leader transition (section 3.1), it is then validated against experimental data on the steady-state negative differential resistance of plasma arcs (section 3.2), and finally, compared to well-established gas-dynamic return stroke simulations (section 3.3). As an application of the model, we simulate optical emissions of rocket-triggered lightning and compare to the experimental findings of Quick and Krider (2017) (section 3.4).

2. Model Formulation

2.1. Basic Equations

In this work we describe the minimal model to qualitatively capture the consequences of the plasma nature of lightning channels. The key simplification here is to solve a set of zero-dimensional equations (i.e., with zero spatial dimensions) that describe the temporal dynamics of the plasma in a given cross section of the channel. Starting from a general 3-D problem, we can progressively reduce the dimensionality of the system. A schematical representation of the model is given in Figure 1a. It can be assumed that the lightning channel is a long cylinder. The axial symmetry indicates that the plasma conditions do not depend on the polar coordinate. Furthermore, the 2-D long cylinder geometry can be reduced to a 1-D radial one, by noting that variations along the channel have significantly larger length scales than along the radial direction. Thus, the change in plasma properties are driven by the conduction current created by the overall lightning tree dynamics and merely imposed in that channel section. Finally, the 1-D radial dynamics can be averaged over to produce self-similar solutions of average channel properties. The minimal set of equations can be written as follows:

$$E = RI = \frac{I}{\sigma \pi r_c^2} = \frac{I}{e\mu_e n_e \pi r_c^2} \tag{1}$$

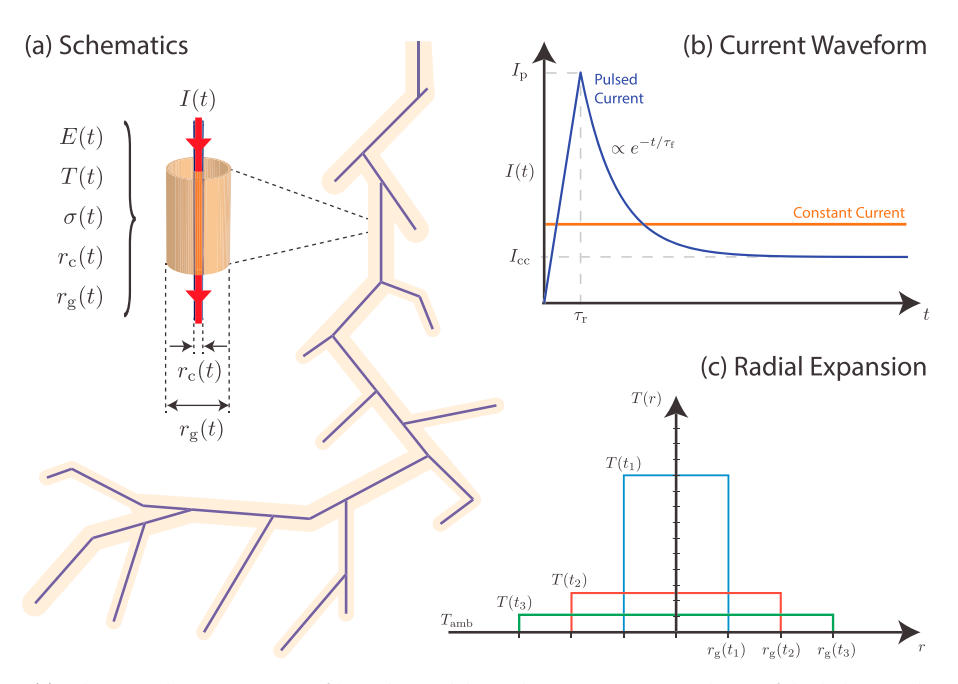


Figure 1. (a) Schematical representation of how the model simulates a cross sectional area of the lightning channel, provided only the current passing through that region I(t) and the channel initial conditions. (b) Current waveforms adopted in this study: constant current versus four-parameter pulsed profile. (c) Radial temperature profile and corresponding channel expansion. Lightning leader channels are surrounded by streamer zones and corona sheaths, which are not depicted in panel (a).

$$\rho_m c_p \frac{\mathrm{d}T}{\mathrm{d}t} = \eta_T \sigma E^2 - \frac{4\kappa_T}{r_\mathrm{g}^2} \left(T - T_\mathrm{amb} \right) - 4\pi\epsilon \tag{2}$$

$$\frac{\mathrm{d}n_{e}}{\mathrm{d}t} = \left(v_{\rm i} - v_{\rm a2} - v_{\rm a3}\right)n_{e} + v_{\rm d}n_{n} + k_{ep}n_{\rm LTE}^{2} - k_{ep}n_{e}\left(n_{e} + n_{n}\right) \tag{3}$$

$$\frac{\mathrm{d}n_n}{\mathrm{d}t} = \left(\nu_{\mathrm{a}2} + \nu_{\mathrm{a}3}\right) n_e - \nu_{\mathrm{d}} n_n - k_{np} n_n \left(n_e + n_n\right) \tag{4}$$

$$\frac{\mathrm{d}r_{\mathrm{c}}^{2}}{\mathrm{d}t} = 4D_{\mathrm{a}} \tag{5}$$

$$\frac{\mathrm{d}r_{\mathrm{g}}^{2}}{\mathrm{d}t} = \frac{4\kappa_{T}}{\rho_{m}c_{p}} \tag{6}$$

Equation (1) is the Ohm's law applied to the channel's cross section, which relates the axial electric field E to the electrical current I, via the resistance per unit channel length $R=1/\sigma\pi r_{\rm c}^2$, where σ is the electrical conductivity and $r_{\rm c}$ is the plasma channel or current-carrying radius. (For the remainder of this manuscript, we refer to the resistance per unit channel length R as simply the resistance.) The electrical conductivity is given by $\sigma=e\mu_e n_e$ under the assumption that only the electron contribution is important, where e is the electronic charge, μ_e is the electron mobility, and n_e is the electron density. This is a reasonable approximation because the ion mobility is of the order of 10^{-4} m $^2 \cdot V^{-1} \cdot s^{-1}$ (at 1 atm), while the electron mobility is 2–4 orders of magnitude larger in the range of typical electric fields present in electrical discharges (see, e.g., Figure 3a).

Equation (2) describes the rate of change of air temperature T, where ρ_m is the air mass density and c_p is the specific heat at constant pressure. The first term on the right-hand side is the rate of Joule heating of air, where $\eta_T \simeq 10\%$ is the fraction of electron Joule heating power contributing to air heating. The second term represents cooling due to heat conduction, where $r_{\rm g}$ is the thermal radius (delimiting the hot air region), κ_T is the thermal conductivity, and $T_{\rm amb} = 300~{\rm K}$ is the ambient air temperature. The third term corresponds to

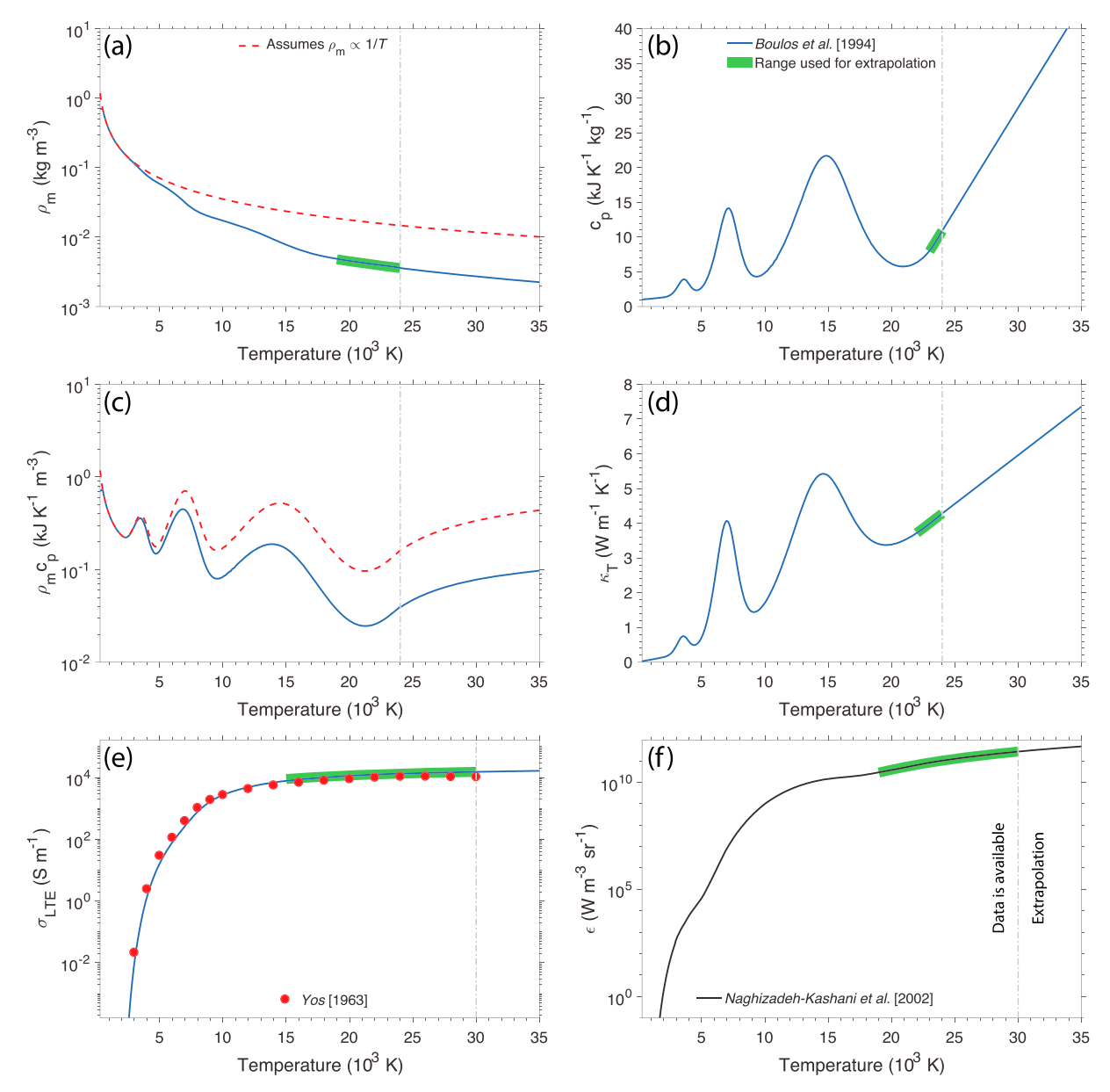


Figure 2. The solid lines show the local-thermodynamic equilibrium (LTE) properties of air as a function of temperature used in the present paper. (a) Mass density ρ_m , (b) specific heat at constant pressure c_p , (c) the product $\rho_m c_p$, (d) thermal conductivity κ_T , (e) electrical conductivity $\sigma_{\rm LTE}$, and (f) net emission coefficient ϵ for an optically thin plasma. The red dashed line in panels (a) and (c) show the ideal gas law trend $\rho_m \propto 1/T$. In the original references, data are only available for temperatures to the left of the vertical dash-dotted line. For higher temperatures, we perform an analytical extrapolation using the data in the range highlighted in green. The air-plasma properties shown in the figure are taken from Boulos et al. (1994, pp. 413–417), unless otherwise noted.

energy loss due to radiative emission, where ϵ is the net radiation emission coefficient. Equation (2) assumes isobaric air heating and neglects cooling by convection.

Equation (3) describes the change in electron density n_e . The first term on the right-hand side describes the rate of change due to field-induced, electron-impact processes, where v_i , v_{a2} , and v_{a3} are the ionization, two-, and three-body attachment frequencies, respectively. The second term describes electron detachment from negative ions, where v_d is the detachment frequency and n_i is the negative-ion density. The third term describes the effective rate of thermal ionization, where k_{ep} is the rate coefficient for electron-positive ion recombination, and $n_{\rm LTE}$ is the electron density in local thermodynamical equilibrium (LTE), defined as $n_{\rm LTE} = \sigma_{\rm LTE}/e\mu_e$. The LTE conductivity $\sigma_{\rm LTE}$ is only a function of temperature (see, e.g., Figure 2e). The fourth



term represents plasma decay due to electron-positive ion recombination. Charge neutrality is assumed; thus, the positive-ion density is equal to $n_e + n_n$.

Equation (4) describes the evolution of an effective or generic negative-ion density n_n . This quantity represents O^- and O_2^- , the dominant negative ions in atmospheric discharges. These species are created by two- (v_{a2}) three-body attachment (v_{a3}) , respectively. The last term in equation (4) represents a sink of negative ions due to negative-positive ion recombination, where k_{np} is the corresponding rate coefficient.

Equations (5) and (6) describe the rate of expansion of the current-carrying radius $r_{\rm c}$ and of the thermal radius $r_{\rm g}$, respectively, where $D_{\rm a}$ is the ambipolar diffusion coefficient. For all purposes, $r_{\rm c}$ represents the discharge channel radius, because it enters in the calculation of Joule heating power deposited in the channel via equation (1). The parameter $r_{\rm g}$ is best interpreted as a measure of the curvature of the radial temperature profile, and its only contribution in the system of equations is in the thermal conduction cooling in equation (2).

The set of six equations (1)–(6) is solved to obtain the temporal dynamics of six unknowns E, T, n_e , n_n , r_g , and r_c , respectively. The input parameters are the source current dynamics I(t) and the initial conditions for the five state variables (T, n_e , n_n , r_g , and r_c), as shown in Figure 1a. The initial value of the electric field is given directly from equation (1).

In order to solve equations (1)–(6), several coefficients are required. These coefficients are a function of E/δ , T, or both. The quantity E/δ is the so-called reduced electric field, where δ is the reduction of air density in comparison to the sea level, room temperature value, defined precisely as $\delta = \rho_m(h,T)/\rho_m(h=0 \text{km},T=300 \text{K})$; h here corresponds to the altitude above mean sea level. Figure 2 shows all LTE plasma coefficients used: (a) ρ_m , (b) c_p , (c) $\rho_m c_p$, (d) κ_T , (e) σ_{LTE} , and (f) ϵ . The LTE parameters are, by definition, only function of temperature. Note that the assumption of isobaric heating combined with the ideal gas law would lead to a dependence $\rho_m \propto 1/T$ between mass density and temperature. This trend is shown in Figures 2a and 2c as a red dashed line. However, in the present work, we use the full equilibrium calculations given by Boulos et al. (1994), shown as blue solid lines in the figure.

Figure 3 shows the field-dependent coefficients: (a) μ_e , (b) effective frequencies of electron production and loss processes, (c, d) recombination coefficients, and (e, f) D_a . The conventional breakdown threshold is defined by the equality between electron-impact ionization (v_i) and two-body attachment (v_{a2}) in Figure 3b. For the coefficients used here its numerical value is $E_k/\delta=28.4$ kV/cm. Figures 3c and 3d show both the electron-positive ion (k_{ep}) and negative-positive ion (k_{np}) recombination coefficients, as a function of the reduced electric field and temperature, respectively. Similarly, Figures 3e and 3f show the ambipolar diffusion as a function of electric field and temperature, respectively.

The coefficients have been obtained from the following references: ρ_m , c_p , and κ_T (Boulos et al., 1994); $\sigma_{\rm LTE}$ (Boulos et al., 1994; Yos, 1963); ϵ (Naghizadeh-Kashani et al., 2002); μ_e (Cho & Rycroft, 1998); v_i and v_{a2} (Benilov & Naidis, 2003); v_{a3} (Morrow & Lowke, 1997); v_d (Luque & Gordillo-Vázquez, 2012); k_{ep} and k_{np} (Kossyi et al., 1992); and D_a is defined by the Einstein relation (Raizer, 1991, p. 20). Both k_{ep} and D_a effectively depend on the electron temperature T_e . The expression for $T_e(E/\delta,T)$ is taken from Vidal et al. (2002). The rate coefficients are given for an air composition of 80% N_2 and 20% O_2 . All rate coefficients used in this manuscript have been summarized in the form of two Matlab functions and made publicly available online (da Silva, 2019a).

2.2. Key Assumptions

1. Externally driven electrical current. A key assumption of the model is that the electrical current is generated by the overall lightning discharge electrodynamics and merely imposed to the channel cross section of interest. This allows one to calculate the channel properties for a given constant or pulsed current waveform. Here we use two types of waveforms: a constant current (in sections 3.1 and 3.2) and a four-parameter pulsed current waveform (in sections 3.3 and 3.4). The pulsed current waveform qualitatively captures most impulsive processes taking place in the lightning channel, and it is given by the following mathematical expression:

$$I(t) = \begin{cases} I_{\rm p} t/\tau_{\rm r} & \text{if} \quad t \le \tau_{\rm r} \\ (I_{\rm p} - I_{\rm cc}) \exp(-t/\tau_{\rm f}) + I_{\rm cc} & \text{if} \quad t > \tau_{\rm r} \end{cases}$$
 (7)

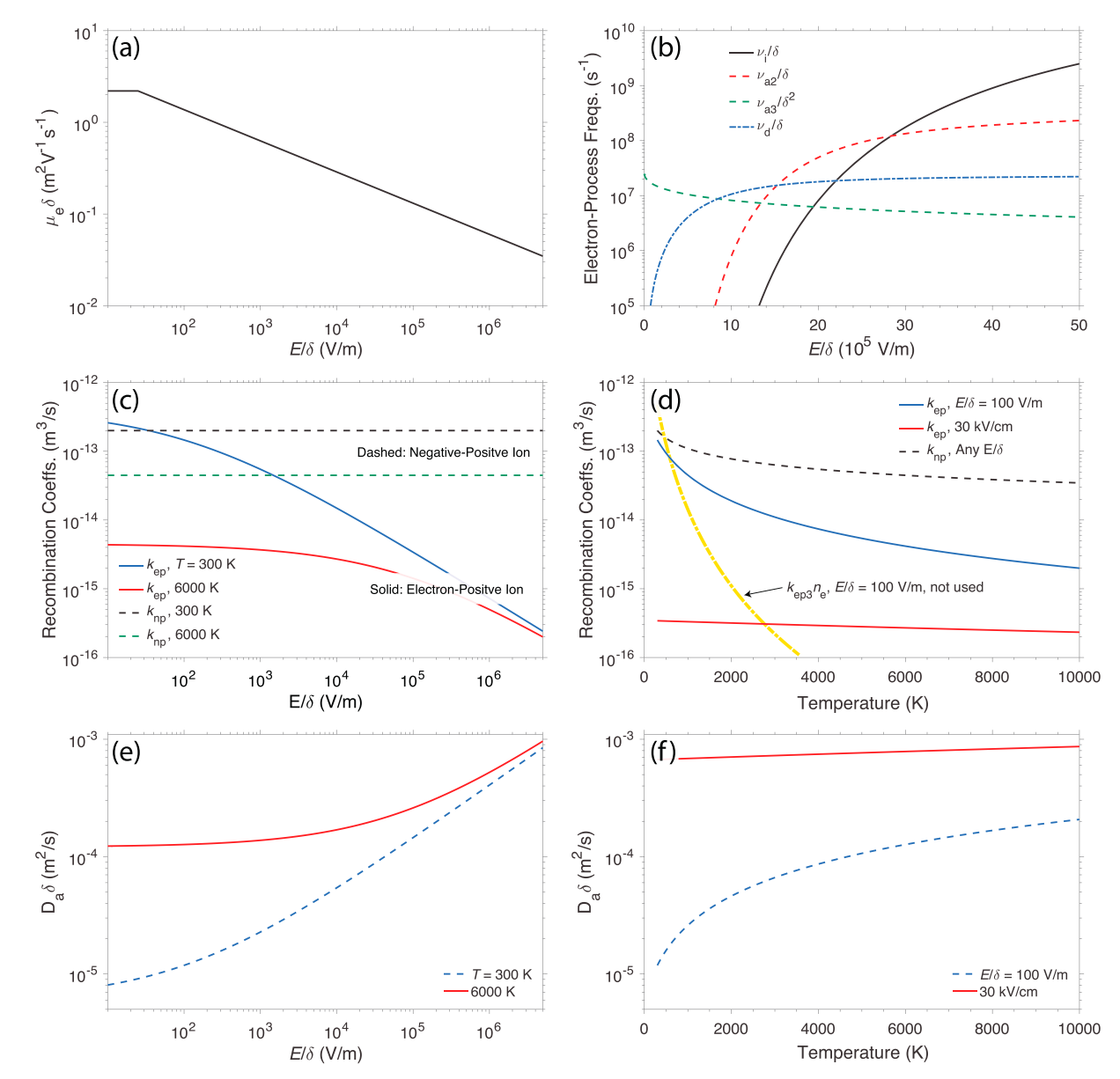


Figure 3. Electric-field-dependent coefficients used in this investigation. (a) Electron mobility μ_e . (b) Effective frequencies of electron production and loss processes v_i , v_{a2} , v_{a3} , and v_d , from equation (3). (c, d) Recombination coefficients k_{ep} and k_{np} . (e, f) Ambipolar diffusion coefficient D_a . Panel (c) shows the recombination coefficients as a function of E/δ for two different temperature values. Contrastingly, panel (d) shows the same coefficients as a function of T for two values of T0. The same strategy is used to display T0 in panels (e) and (f). Panel (d) also shows the rate coefficient for three-body electron-positive-ion recombination (electrons are the third body), or more precisely T0 in panels (e) T1. This process is not included in the model, and the coefficient is just shown for comparison with the two-body rate. Expressions for the rate coefficients shown in this figure are given by da Silva and Pasko (2013); see text for references

The four parameters in the waveform are peak current $I_{\rm p}$, rise time $\tau_{\rm r}$, fall time $\tau_{\rm f}$, and continuing current $I_{\rm cc}$. These four parameters can be adjusted to represent a first or subsequent return stroke with or without continuing current. They can also be adjusted to allow the model to simulate the surge current injected in the leader channel following the stepping process (see, e.g., Winn et al., 2011), a dart leader reionization wave, or ICC pulses happening during the initial continuous current (ICC) stage of a rocket-triggered lightning flash. A schematical representation of this waveform is given in Figure 1b. It should be noted that several different analytical functions have been used to simulate the current waveform propagating through the lightning channel, such as the Heidler function (Heidler, 1985; Rakov & Uman, 1998), the double exponential (Bruce & Golde, 1941), or the asymmetric Gaussian (e.g., da Silva et al., 2016). The model



can handle any of them as input; equation (7) is chosen for its simplicity and to facilitate the comparison with the work of Plooster (1971) and Paxton et al. (1986) in section 3.3 below.

The overall strategy of prescribing I(t) and calculating the channel properties has been successfully employed by a number of researchers to investigate the dynamics of streamer-to-leader and streamer-to-spark transition (Aleksandrov et al., 2001; da Silva & Pasko, 2012; Gallimberti et al., 2002; Popov, 2003) and to simulate the channel decay following a return stroke (Aleksandrov et al., 2000; Hill, 1971; Paxton et al., 1986; Plooster, 1971). Although insightful, this strategy does not reveal the full lightning electrodynamics, because changes in the plasma conductivity should feedback into how much current is flowing in the channel. However, the approach used here allows us to provide a detailed characterization of the plasma-channel nonlinear resistance R(t) for a given current I(t). This manuscript should be seen as an initial effort toward quantifying the effects of the nonlinear plasma resistance into the overall electrodynamics of lightning leaders. Future investigations can leverage this model by replacing equation (1) with lumped or distributed circuit equations that describe the lightning discharge tree.

- 2. Averaged radial dynamics. The radial profile of temperature is assumed to follow a step function so that T(r) = T for $r \le r_{\rm g}$ and $T(r) = T_{\rm amb}$ for $r > r_{\rm g}$. The radial expansion is given by an increase of $r_{\rm g}$ at a rate given by equation (6). It is assumed here that the expansion rate is determined by thermal conduction or, in other words, the radial temperature profile follows the equation $\partial T/\partial t = k\nabla^2 T$, where $k = \kappa_T/\rho_m c_p$. The solution for this equation under a delta function initial condition is $T(r,t) = \exp(-r^2/4kt)/\sqrt{4\pi kt}$. The solution is a Gaussian function with half-width $r_{\rm g} = \sqrt{4kt}$. Taking the time derivative of this expression, one obtains the expansion rate of the thermal radius in equation (6).
 - The second term in the right-hand side (rhs) of equation (2) is the spatially averaged Laplacian of temperature, that is, the rhs of the heat conduction equation. The method for evaluating that term is illustrated in Figure 1c. It is assumed that the thermal conduction-driven expansion conserves the area under the curve in Figure 1c, or the quantity $A = (T T_{\rm amb})\pi r_{\rm g}^2$. Therefore, $\partial T/\partial t|_{\rm conduction}^{\rm thermal}$ is determined from setting $\partial A/\partial t = 0$. This is a rather robust assumption since it is virtually equivalent to enforcing energy conservation. However, in reality, the shape of the profile is not preserved as assumed here.
 - Similar results are obtained by assuming that the plasma distribution expands with ambipolar diffusion, leading to the expansion rate given in equation (5). In this case, the conserved quantity is $A = n_e \pi r_c^2$, or simply the number of electrons per unit channel length. Conservation of A in this case is equivalent to conservation of mass. This analysis also yields a radially averaged ambipolar diffusion sink term in equation (3). However, this loss process is negligible in comparison to chemically driven losses and, therefore, it is not included in equation (3). Our considerations here are similar to Braginskii's (1958), where the plasma channel boundary is assumed to behave as a moving piston that "snowplows" the ambient gas. Both models yield a channel radius expansion as $r_c \propto \sqrt{t}$, but Braginskii's expansion rate is not determined by ambipolar diffusion. In a comparison between several semiempirical models of the lightning return stroke resistance, De Conti et al. (2008) concluded that the model accounting for channel expansion $r_c \propto \sqrt{t}$ effects in the resistance yielded the most robust return stroke radiated electromagnetic field signatures.
- 3. Thermal ionization rate. At temperatures of several thousand Kelvin, the plasma-channel composition is roughly made of equal parts electrons and NO+ ions (Aleksandrov et al., 1997; da Silva & Pasko, 2013; Popov, 2003). The NO+ ions are formed by associative ionization of N and O atoms at a rate $F = k_{\rm assoc} n_{\rm O} n_{\rm N}$. The plasma density is dictated by a balance between associative ionization and electron-positive ion recombination, that is, by $F = k_{ep} n_e n_{\rm NO}^+ \approx k_{ep} n_e^2$. Without knowing the precise rate F, we know that at high temperatures this equation should yield the LTE conductivity given in Figure 2e, or the corresponding electron density $n_{\rm LTE} = \sigma_{\rm LTE}/e\mu_e$. This can be achieved by setting the rate of thermal (associative) ionization to be equal to $F = k_{ep} n_{\rm LTE}^2$, as done in equation (3).
 - Therefore, equation (3) is designed to essentially have two different modes of operation. At low (near-ambient) temperatures, the plasma population balance is driven by electron-impact ionization, attachment, and detachment, that is, the typical chemistry considered in the streamer breakdown of short air gaps (da Silva & Pasko, 2013; Flitti & Pancheshnyi, 2009; Liu & Pasko, 2004; Naidis, 2005; Pancheshnyi et al., 2005). However, at high temperatures (\gtrsim 10,000 K) the equation yields the LTE conductivity $\sigma_{\rm LTE}(T)$, in alignment with the typical approach used for the simulation of free-burning arcs (Chemartin et al., 2009; Lowke et al., 1992) or used in gas-dynamic return stroke simulations (Aleksandrov et al., 2000; Paxton et al., 1986; Plooster, 1971). It is not possible to state exactly what is the minimum temperature at which the assumption of LTE regime yields accurate calculations. Both T and T_e depend on the history of



energy deposition and losses in the channel, which in its turn depend on the electric field and the electron density. In this manuscript, we loosely give the value of 10,000 K as an estimate. This is the value at which the electron temperature is only 5% and 50% larger than the neutral gas one for electric fields of 10 and 1000 V/m, respectively. In the present work, the electron temperature is obtained under the assumption that the electron energy balance equation is in steady state. Therefore, yielding the simple relation $T_e = T + f(E/\delta)$, where the function $f(E/\delta) \propto (E/\delta)^{0.46}$ is taken from Vidal et al. (2002). Essentially, this equation asserts that the non-equilibrium results from the presence of an electric field in the discharge plasma and that equilibrium is only achieved when E = 0.

In some types of plasmas the high-temperature density is given by a balance between electron impact ionization (driven by high T and not high E/δ) and three-body electron-positive ion recombination (electrons are the third body). One such example are Argon arc discharges at atmospheric pressure (see, e.g., Sansonnens et al., 2000; Tanaka et al., 2003). In this case, plasma losses would happen at a rate $\approx k_{ep3} n_e^3$, and using the assumptions discussed in the last two paragraphs, the plasma production rate would be $\approx k_{ep3} n_{\rm LTE}^3$, where k_{ep3} is the three-body electron-positive ion recombination rate coefficient given in units of m⁶/s. Owing to the cubic power law dependence, three-body electron-positive ion recombination is important when the plasma density is high. In this work, we assume that the high-temperature balance is given by the two-body processes, because they are the dominant ones in the temperature range between 2,000-9,000 K (i.e., in the transition to LTE regime), as discussed by Bazelyan and Raizer (2000, pp. 75-80) and Aleksandrov et al. (2001). To verify that this assumption is true, we first plot the rate coefficients $k_{ep} \propto T_e^{-1.5}$ and $k_{ep3} \propto T_e^{-4.5}$ in Figure 3d with rate coefficients taken from Kossyi et al. (1992) for an air plasma. Figure 3d actually shows $k_{ep3}n_e$ so that the units match, with $n_e = 10^{20}$ m⁻³, a typically large value in our simulations. It can be seen that due to the weaker fall off with temperature, two-body recombination increasingly dominates over three-body in the temperature range of interest. Second, we show later in section 3.3 quantitative comparisons between the two rates for specific simulation results obtained with our model, further justifying our use of two-body process rates.

- 4. Negative ion chemistry. Equation (4) describes the evolution of an effective or generic negative-ion density n_n , representing O^- (created by two-body attachment) and O_2^- (created by three-body attachment), the dominant negative ions in ambient-temperature discharges. In the hot lightning channel, negative ions disappear, and the plasma composition is given by a balance of positive ions and electrons. By comparing equations (3) and (4), we can see that attachment works as a sink in the former, but as a source in the latter. Detachment plays the opposite role. Therefore, the attachment-detachment cycle does not represent a true plasma loss. Effectively, electrons can be thought to be temporarily stored in negative ions to be released at a later time, after substantial accumulation. It is assumed here that O_2^- created by three-body attachment quickly converts into O_2^- in collisions with atomic oxygen favored by elevated temperatures in the lightning channel (da Silva & Pasko, 2013, Figure 11a). Therefore, detachment is dominantly driven by collisions between O_2^- and O_2^- (Luque & Gordillo-Vázquez, 2012; Rayment & Moruzzi, 1978). These assumptions allow us to account for effects of negative-ion chemistry in a simple yet reasonably accurate manner.
- 5. Fast air heating. The coefficient η_T in the first term on the rhs of equation (2) is the fraction of electronic power (or Joule heating rate σE^2) that is directly transferred into random translational kinetic energy of neutrals and, thus, contributes to air heating. This quantity has been calculated to be $\eta_T \simeq 0.1$ at near-ambient temperatures (da Silva & Pasko, 2013; da Silva, 2015), largely arising from surplus energy from the quenching of excited electronic states and molecular (electron-impact) dissociation, which consist the so-called fast air heating mechanism (Popov, 2001, 2011; da Silva & Pasko, 2014). Most of the remainder electronic power is spent into the excitation of vibrational energy levels of nitrogen molecules. However, as temperature increases, rates of vibrational-translational energy relaxation quickly accelerate, effectively making $\eta_T \approx 1$ for temperatures of 2,000 K and above (provided that radiative losses are treated in a separate sink term in the rhs of the energy balance equation). This delayed vibrational energy relaxation is typically described with an extra equation for the total vibrational energy of N_2 molecules. In the present work, we capture this phenomenology, without the need for an extra equation, by adopting a parametric dependence of η_T on temperature, given by $\eta_T = 0.1 + 0.9 [\tanh(T/T_{amb} 4) + 1]/2$. The added second term in this expression simulates the acceleration of vibrational energy relaxation, yielding $\eta_T = 1$ for T > 2,000 K with a smooth ramp transition between 1,000–1,500 K.



3. Results and Discussion

3.1. Streamer-to-Leader Transition

The most fundamental step in the formation of a lightning channel is the streamer-to-leader transition. Streamers are the precursor stage. They are thin filamentary discharge channels that propagate as a non-linear electron-impact ionization wave, self-enhancing the electric field at its tips. Their conductivity is of the order of 0.1-1 S/m. They require electric fields higher than 17% of the conventional breakdown threshold for stable propagation. Streamer lifetimes are rather short, approximately tens of microseconds, limited by attachment to oxygen molecules. Leaders are a necessity for the breakdown of air gaps longer than one meter (Bazelyan & Raizer, 2000, p. 59). It takes several milliseconds for a leader to come from the cloud to the ground. The only way to keep the leader channel conductive for so long is by substantially heating the air. In the hot air plasma, attachment loses its importance; instead, the electron density decays via electron-positive ion recombination, which is substantially slower. The transition between streamer and leader happens in a region in space called stem, a converging point where several streamers in a streamer corona are rooted. In this region the small current carried by individual streamers can add up to values $\gtrsim 1$ A to produce air heating and create a leader channel.

da Silva and Pasko (2013) developed a first-principles model to investigate the dynamics of streamer-toleader transition. It consists of four main blocks: (1) a set of fully nonlinear gas-dynamic equations that described the heating and radial expansion of the neutral gas; (2) a detailed kinetic scheme accounting for the most important processes in an air discharge plasma; (3) energy exchange between charged and neutral particles accounting for the partitioning of electronic power between elastic collisions, and excitation of vibrational and electronic states; and (4) delayed vibrational energy relaxation of nitrogen molecules. da Silva and Pasko's (2013) model was validated against streamer-to-spark transition time scales measured in centimeter-long laboratory discharges (Černák et al., 1995; Larsson, 1998). That model was also applied to simulation of leader speeds at reduced air densities and for interpretation of the phenomenology of gigantic jets (da Silva & Pasko, 2012), as well as to study the mechanism of infrasound emissions in sprites (da Silva & Pasko, 2014). Figure 4a shows, as discontinuous traces, the air heating rate calculated with da Silva and Pasko's (2013) model with an assumed Gaussian initial distribution of electron density in the streamer channel. The peak n_e value is 2×10^{20} m⁻³ and the e-folding spatial scale is $r_c = 0.3, 0.5, \text{ and } 1$ mm, respectively. The streamer-to-leader transition time scale τ_h is defined as the time required to heat the channel up to 2000 K; the heating rate shown in the figure is simply $1/\tau_h$. The 2000-K threshold is chosen because when the channel reaches this temperature level a thermal-ionizational plasma instability is triggered: vibrational relaxation is accelerated, temperature raises very sharply, N + O associative ionization starts to take place, and transition to leader mode is unavoidable.

The present work's goal is to propose the minimal physical model to describe the dynamics of the leader plasma. As discussed in section 2.2, the model uses a simplified plasma chemistry and parameterized radial dynamics. As a means of validation, in Figure 4 we compare the present model with the simulations of da Silva and Pasko (2013). Figure 4a uses the same initial conditions as the previous work and an initial current-carrying radius $r_c = 0.5$ mm. The figure shows order-of-magnitude agreement between the two models. However, there is an inherently different slope between the two curves, attributed to the multiple parameterizations and simplifications introduced in this paper. The other three panels in the figure show the effects of the initial conditions in the air heating rate: n_e (b), r_c (c), and r_g (d). The current-carrying radius is the parameter that has the largest influence on the heating rate (Figure 4c). The thermal radius $r_{\rm g}$ has no effect on the heating rate at all (Figure 4d), because this quantity is exclusively related to the cooling rate of the channel (see equation (2)), which is negligible in submicrosecond time scales. The dependence on initial electron density is slightly more complicated. The heating rate is $\propto \int_0^{\tau_h} \sigma E^2 dt$ which, according to equation (1) is also $\propto \int_0^{\tau_h} I^2/n_e dt$. The inverse $1/n_e$ dependence can be qualitatively seen when comparing the 10²⁰- and 10²²-m⁻³ cases. But reducing the initial electron density tends to increase the electric field according to Ohm's law. If the electric field goes beyond E_k , ionization increases n_e until the field drops down to the E_k level. This self-regulatory mechanism imposes a maximum heating rate given by the 10^{18} to 10^{20} -m⁻³ curves in Figure 4b.

For the sake of comparison, we have repeated the calculations shown here with a full LTE version of the model. This is done by replacing equations (3) an (4) with $\sigma = \sigma_{\rm LTE}$ and by setting $\eta_T = 1$. The calculated air heating rate is in the range of 10^{12} – 10^{15} s⁻¹ for currents between 1 and 100 A. They are not shown in Figure 4 because they lie completely outside of the vertical-axis limits. This result indicates that a full-LTE

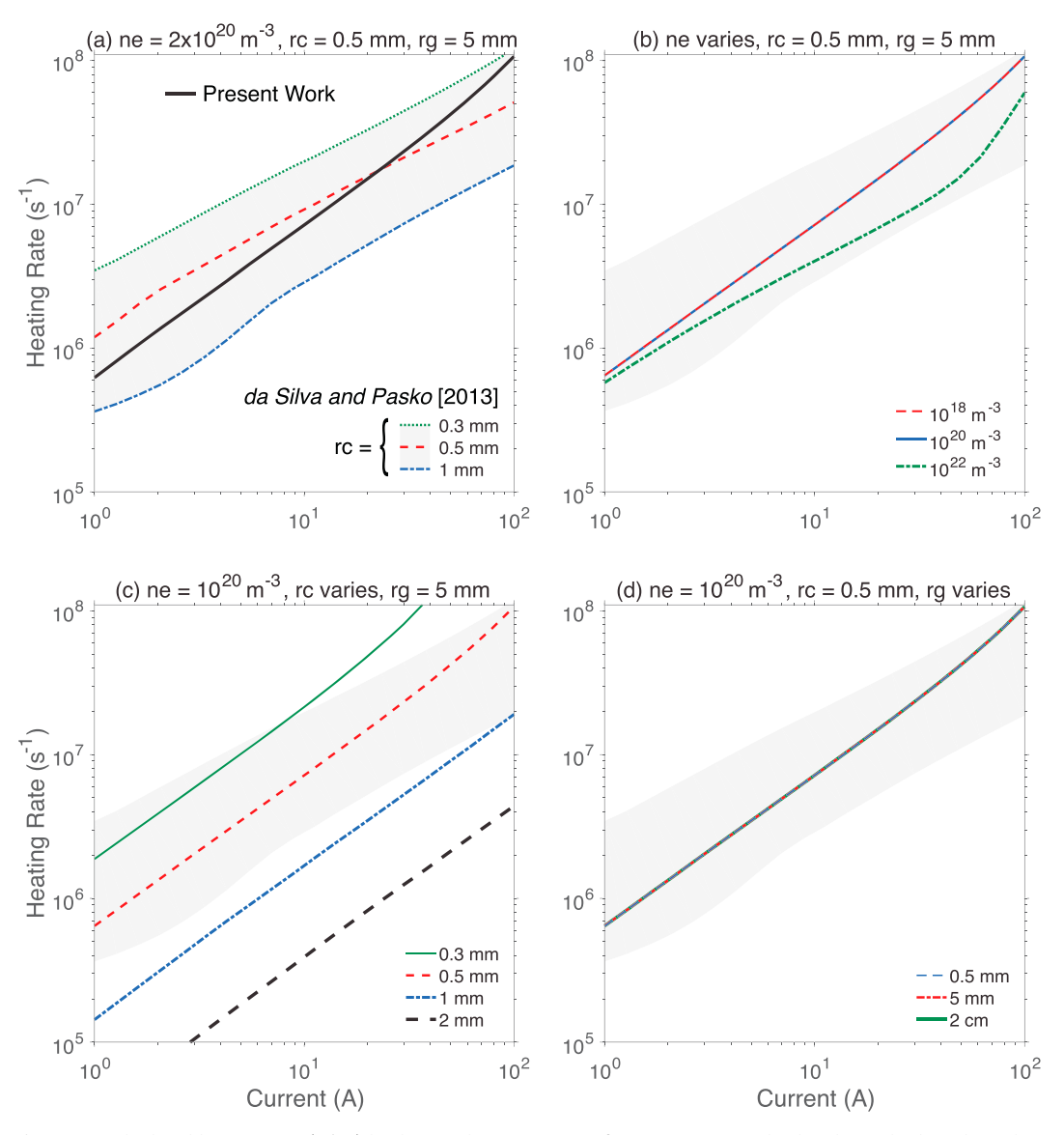


Figure 4. Calculated heating rate $(1/\tau_{\rm h})$ leading to the conversion of a streamer into a leader channel. The title in the four panels list the initial conditions for electron density n_e (ne in the figure), current-carrying radius $r_{\rm c}$ (rc), and thermal radius $r_{\rm g}$ (rg) used in the simulations. The ambient neutral temperature is 300 K, and there are no negative ions initially. Panel (a) shows as discontinuous traces the calculation of da Silva and Pasko (2013) for the same initial conditions, but three different values of r_c . The gray shaded area delimiting the calculations of da Silva and Pasko (2013) is repeated in all four panels for comparison. Panels (b)–(d) emphasize the effect of changing the initial conditions for n_e (b), $r_{\rm c}$ (c), and $r_{\rm g}$ (d).

model completely overestimates the air heating rate, and cannot capture the finite streamer-to-leader (or to-spark) transition time scale, well known from laboratory studies to be a fraction of 1 μ s (Černák et al., 1995; Larsson, 1998). The reason for the unreasonably high air heating rate of a full-LTE model lies in the fact that the LTE conductivity at 300 K is substantially lower than the typical conductivity in a streamer channel (see Figure 2e). Since conductivity is lower, the resistance per unit length R is larger, and so is the Joule heating rate RI^2 , which is the same argument presented when discussing Figure 4b.

In summary, the present model compares very well to a first-principles theoretical simulation that has been validated with spark data from laboratory discharges. The proposed computer-simulation tool is able to account for the finite time scale of streamer-to-leader transition, something that a full-LTE model cannot. The following input parameters are used as initial conditions in all simulations below, unless otherwise noted: $n_e = 10^{20} \; \mathrm{m}^{-3}$, $r_c = 0.5 \; \mathrm{mm}$, $r_g = 5 \; \mathrm{mm}$, $n_n = 0$, $T = 300 \; \mathrm{K}$.

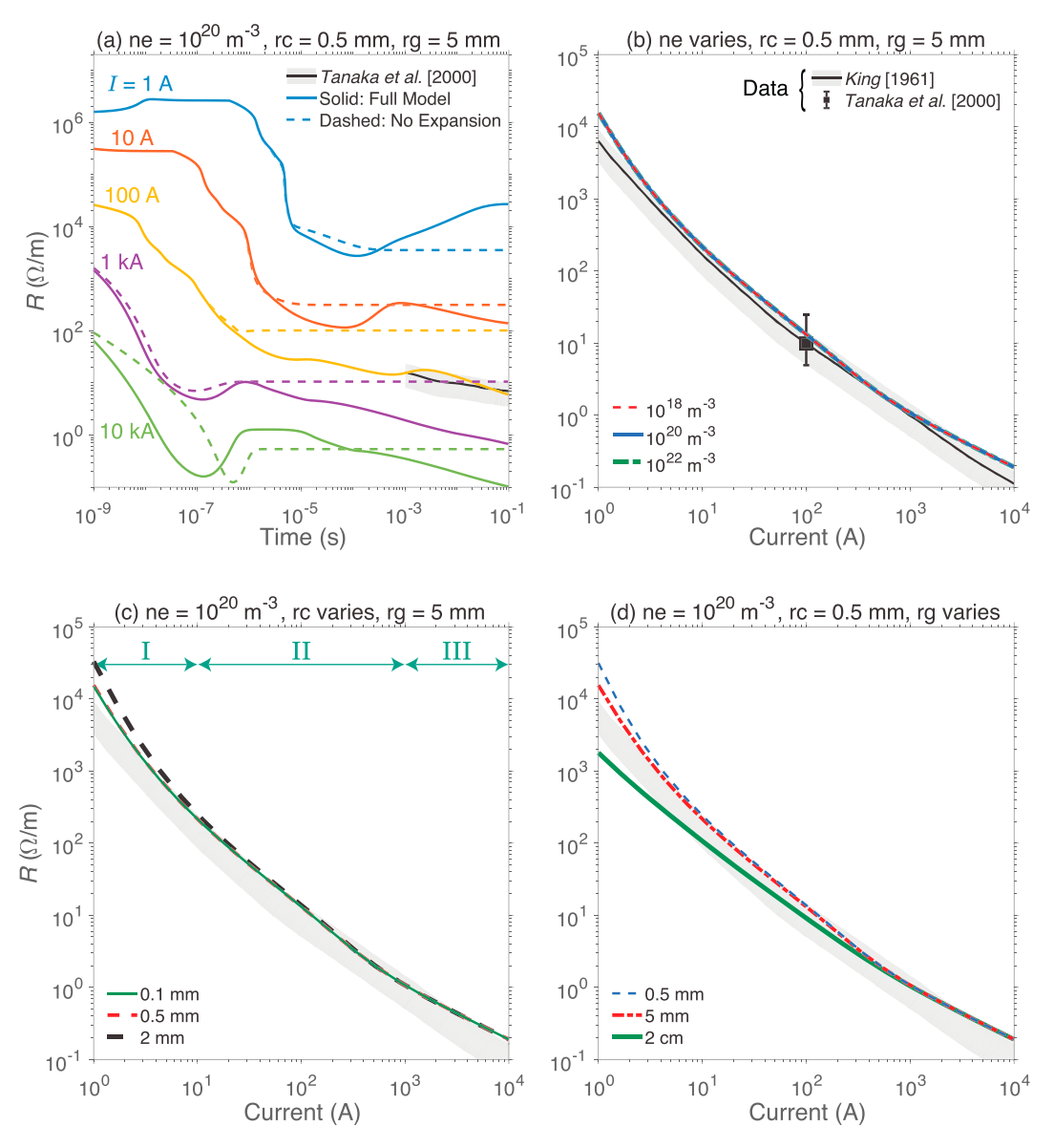


Figure 5. (a) Temporal dynamics of resistance in a discharge channel for several current values. Solid and dashed lines show the contrast between full model versus suppressed channel expansion, respectively. The figure also shows the data by Tanaka et al. (2000) as a solid black line, with the gray shaded area marking $\pm 50\%$ variability. (b–d) Resistance value at 10 ms as a function of current. Panel (b) also shows the data from Tanaka et al. (2000) at 10 ms (square with $\pm 50\%$ error bar), as well as, the steady-state arc resistance measured by King (1961) (black solid line with $\pm 50\%$ gray shaded band). Panels (b)–(d) emphasize the effect of changing the initial conditions for n_e (b), r_c (c), and r_g (d), with the initial conditions being listed in the panel titles and legends. The gray shaded band marking the results from King (1961) are repeated in panels (b-d) for comparison with our simulations.

3.2. Steady-State Negative Differential Resistance

The behavior of the steady-state resistance of arc channels has been used to discuss the phenomenology of lightning channels (Hare et al., 2019; Heckman, 1992; Krehbiel et al., 1979; Mazur & Ruhnke, 2014; Williams, 2006; Williams & Heckman, 2012; Williams & Montanyà, 2019). Steady-state plasma arcs exhibit the so-called negative differential resistance, that is, the resistance decreases with increasing electrical current. Such behavior is reproduced in our simulations and shown in Figure 5. Figure 5a shows the temporal evolution of resistance in the discharge channel for several values of electrical current between 1 A and 10 kA. It is easy to see that, owing to channel expansion, there is no true steady-state resistance. A constant value for the steady-state resistance can only be obtained if channel expansion is suppressed (compare the solid and dashed lines). At low currents (see the 1-A curve), one can start to see the channel recovery

Table 1							
Fit Parameters for the Resistance per Unit Channel Length Formula $R = A/I^b$							
Reference	Current range (A)	Time scale (s)	$A\left(\Omega \mathrm{A}^b/\mathrm{m}\right)$	b	Mean fit error (%)		
This Work	10^{0} – 10^{4}	10^{-2}	4.27×10^3	1.18	35		
This Work	$10^0 - 10^4$	1	4.81×10^{3}	1.37	74		
This Work: Region I	10^{0} – 10^{1}	10^{-2}	1.24×10^4	1.84	9		
This Work: Region II	$10^1 - 10^3$	10^{-2}	2.82×10^{3}	1.16	4		
This Work: Region III	$10^3 - 10^4$	10^{-2}	0.18×10^3	0.75	1		
King (1961)	$10^0 - 10^4$	_	2.87×10^{3}	1.16	25		
Bazelyan and Raizer (1998)	_	_	3×10^{4}	2	_		

starting as early as 0.1 ms. The recovery in this case is due to the fact that the channel cools down to a sufficient level that three-body attachment becomes important, accelerating the rate of plasma density depletion. For currents higher than 10 A, the resistance is still decreasing at the 0.1 s mark; in some cases after a partial recovery. In Figure 5a we also show data from Tanaka et al. (2000) used by Chemartin et al. (2009) to validate their 3-D free burning arc simulations. Tanaka et al. (2000) report on 1.6-m-long arcs with 100-A current. Their measurements are shown in Figure 17 of Chemartin et al. (2009). We obtain a good agreement between our simulations and the measurements despite the fact that the 3-D tortuous nature of the arc channel is neglected in the present work.

For the purpose of evaluating the negative differential resistance behavior predicted by our simulations, we evaluate the resistance (per unit length) at 10 ms for several different values of electrical current. The results are shown in Figure 5b alongside measurements from King (1961). We chose to compare our simulations to King's measurements because this work has been featured in a number of manuscripts in lightning-research literature (e.g., Heckman, 1992; Mazur & Ruhnke, 2014; Williams, 2006; Williams & Heckman, 2012). The data from King (1961) is shown as a black solid line with a ±50% variability gray shaded band. The gray band is repeated in panels (b)-(d) for comparison with our simulations. The time instant of 10 ms is chosen because it is when the time-dependent data from Tanaka et al. (2000) (shown as a square with ±50% error bar) best aligns with King's curve. Our calculations in Figure 5a show good agreement with King's curve; the average difference between the two is 40%. Figures 5b-5d show the effects of the initial conditions in the steady-state resistance: n_e (b), r_c (c), and r_g (d). It can be seen that changes in the initial conditions have very little impact on the resistance in the 10-ms time scale. It is as if the channel "forgets" the initial conditions (Aleksandrov et al., 2001). Given the uncertainty in determining the initial conditions of the channel, this result lends robustness to the resistance calculations shown hereafter. However, in shorter time scales the resistance R does depend on the initial conditions. Similarly to the discussion in section 3.1, the dependence on n_e and r_g is weak, but the dependence on r_g can be more noticeable. The dependence on the initial channel radius becomes weaker and weaker at higher currents. As an example, at the 10-µs mark, we find that the ratio $R(r_c=2 \text{ mm})/R(r_c=0.5 \text{ mm})$ is of the order of 700 for a constant current of 10 A. The same ratio is only 0.63 for a current of 1,000 A.

The dependence of the resistance on electrical current can be approximated by the analytical formula $R = A/I^b$, where A and b are positive constants. It is easy to see that with this dependence $\mathrm{d}R/\mathrm{d}I < 0$ always, in accordance with the terminology "negative differential resistance." The limiting case b = 1 corresponds to a constant steady-state electric field inside the channel (with numerical value equal to A). We have evaluated the fit parameters that best match our model for the standard set of initial conditions (shown in the title of Figure 5a). The results are shown in Table 1 alongside the fit parameters for the King's curve and also values given by Bazelyan and Raizer (1998). It can be seen that the exponent b that best fits both the present work and King (1961) are very close to each other (b = 1.16-1.18). The empirical trend given by Bazelyan and Raizer (1998) has a substantially steeper slope (b = 2). If we run the simulation for a longer time, up to 1 s, the power law index increases from 1.18 to 1.37 (see second row in Table 1). However, the mean fit error doubles indicating that the curve deviates further from the power law approximation.

It can be seen from Table 1 that fitting the power law dependence to a four-decade current range produces errors of 35–74%. A better fit can be produced by braking down the current range in three regions: (I) 10^0 – 10^1 A, (II) 10^1 – 10^3 A, and (III) 10^3 – 10^4 A. The three regions are marked in Figure 5c. It can be seen in Table 1



that the three regions have different power law indexes, progressively lower as current increases. Detailed analysis of the temporal evolution of energy deposition in the channel reveals that the steady state is given by different mechanisms in the three regions. In Region I the steady state is given by a balance of Joule heating and heat conduction, that is, between the first and second terms in the right-hand side of equation (2). Meanwhile, In Region III the steady state is given by a balance with radiative emission, that is, between the first and third terms in the right-hand side of equation (2). Region II is marked by a comparable role between the two loss processes; radiative emission is important in the submillisecond time scale, while heat conduction is significant at later stages.

3.3. Energy Deposition in Return Strokes

The return stroke follows the attachment of lightning leader channels to ground structures. In the case of a negative cloud-to-ground discharge, the return stroke effectively lowers several coulombs of negative charge originally deposited along the downward propagating stepped leader. The high-current return stroke wave (with typically tens of kiloamperes) rapidly heats the channel to peak temperatures of the order of 30,000 K, emitting intense optical radiation, and creating a channel expansion shock wave (that produces audible thunder). According to Rakov and Uman (1998), models that describe the lightning return stroke can be divided into four categories: gas-dynamic or physical, electromagnetic, distributed-circuit, and engineering models. The basic set of equations described in this manuscript fits into the first category, where the current flowing through the channel is an input parameter and all other channel properties can be calculated from first principles. Some of the most well-accepted investigations within this framework are the papers by Plooster (1971) and Paxton et al. (1986). These authors solve the hydrodynamic equations of motion for atmospheric-pressure air in a Lagrangian frame of reference. A description of this simulation approach, which shows contemporary versions of the pertinent equations, is given by Aleksandrov et al. (2000). The model resolves the 1-D radial profiles of all state variables and captures the shock wave expansion as driven by ohmic heating. The plasma is assumed to be in LTE and the conductivity is simply $\sigma = \sigma_{\text{LTE}}(T)$. These models also describe the radial transport of radiation, and primarily differ by its implementation and comprehensiveness. Plooster (1971) used a single temperature-independent opacity to obtain radiation loss and absorption in each radial grid point, while Paxton et al. (1986) used a detailed multigroup radiative transport algorithm using a diffusion approximation. A detailed discussion on plasma radiative transport is given by Ripoll et al. (2014a).

In Figure 6a we present a comparison between our model's results and the seminal works of Plooster (1971) and Paxton et al. (1986). The current waveform has the qualitative shape depicted in Figure 1b, with a rise time of 5 μ s and a fall time of 50 μ s (or simply written as 5/50 μ s). The peak current is 20 kA, a typical value for first return strokes, and no continuing current is incorporated. The current waveform is the same one used in the two papers for the simulation case shown in Figure 8 of Paxton et al. (1986). We generate initial conditions by starting the simulation with the standard streamer-like channel parameters used in section 3.1 and running a constant 10-A current through the channel during 4 μ s. This strategy ensures that the channel has the properties of a leader discharge prior to the return stroke. These initial conditions are $r_c = 1$ mm, $r_g = 1$ cm, $n_e = 9 \times 10^{17}$ m⁻³, and T = 5000 K. Additionally, instead of using the value of $\rho_m(T = 5000\text{K})$ for the air mass density, the ambient value $\rho_m(T = 300\text{K}) = 0.7$ kg/m³ is used. These initial conditions are very similar to the ones used in the aforementioned references. Note that even a steady current as low as 10 A can produce a leader with temperature of ~5,000 K. This value is within the estimate for the predart and postdart leader channel temperatures provided by Rakov (1998), which are 3,000 K and 20,000 K, respectively. It can be seen from Figure 6a that our model compares very well with simulation results of Plooster (1971), predicting a peak temperature of 36,000 K. The mean difference between the two curves is 3%.

Both curves (Plooster's and ours) deviate from the results of Paxton et al. (1986). It can be seen from Figure 6a that a better agreement with Paxton et al. (1986) can be found by simply multiplying the radiative emission coefficient (last term in equation (2)) by a factor of 10. This fact can be better understood by looking at the energy deposition in the return stroke channel, depicted in Figure 6b. The figure shows (in order) the four terms in the energy equation (2): the internal energy is given by $\rho_m c_p T \pi r_c^2$, the Joule heating by $\int \eta_T \sigma E^2 \pi r_c^2 dt$, the thermal conduction by $\int \frac{4\kappa_T}{r_c^2} \left(T - T_{\rm amb}\right) \pi r_c^2 dt$, and the radiative emission by $\int 4\pi \epsilon \pi r_c^2 dt$. It can be seen that the channel's temperature is dictated by a balance between Joule heating and cooling by radiative emission. Therefore, simply increasing the rate of channel cooling by radiation can lower the peak temperature and provide a better agreement with Paxton's results. As mentioned above, the models pre-

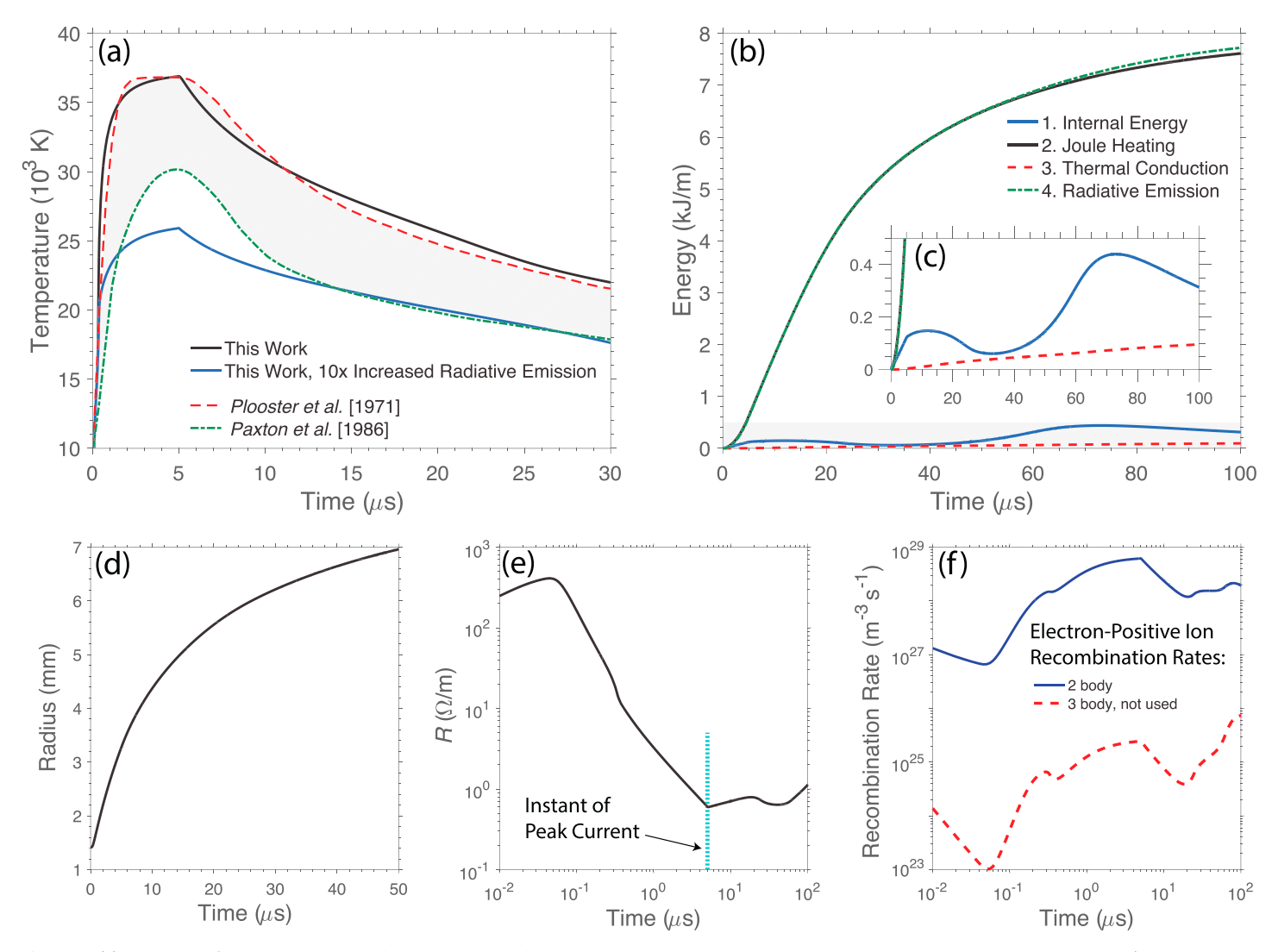


Figure 6. (a) Evolution of temperature in a 20-kA return stroke channel: comparison between the present investigation and established results (Paxton et al., 1986; Plooster, 1971). (b) Energy deposition in the return stroke channel. The four lines, in the order listed in the figure legend, correspond to the four terms in the energy balance equation (2). Panel (c) is a zoom-in into the gray shaded rectangle in panel (b). Panels (d)–(f) show the radius, resistance per unit length, and rates of electron-positive ion recombination, respectively. Panel (f) justifies a posteriori neglecting the three-body process in equation (3).

sented by Plooster (1971) and Paxton et al. (1986) are essentially the same and only differ by the treatment of radiative emission, lending further credence to the idea that peak temperatures are dictated by radiative emission.

An important conclusion to be drawn here is that the effective representation of the radiative emission through a net emission coefficient (ϵ in Figure 2f) produces a proper description of the channel temperature dynamics, especially because all four curves in Figure 6a have similar qualitative shape and rate of cooling after the peak. Moreover, at 35 µs the total deposited energy in our simulations of 5.6 kJ/m compares well to the estimates of 2 and 3.8 kJ/m by Plooster (1971) and Paxton et al. (1986), respectively (see also Rakov & Uman, 1998, Table I). The state of the art in lightning spectroscopy is the recent investigations by Walker and Christian (2017, 2019). From the ratio of several atomic spectral lines recorded with 1-µs temporal resolution, these authors report peak temperatures ranging between 32 and 42 kK for five rocket-triggered lightning strikes with peak currents varying between 8.1 and 17.3 kA (Walker & Christian, 2019, Figure 4). There is not a clear linear correlation between peak current and peak temperature in their dataset and the average peak temperature between the five strikes is $\approx 36\pm4$ kK. Remarkably, our work and Plooster's do a better job reproducing the measured peak temperatures than Paxton's. Further work is required to explain the highest value registered by Walker and Christian (2019), in excess of 42,000 K.



Figure 6d shows the channel radius as a function of time. We have verified that the proposed averaged radial dynamics qualitatively captures the radial expansion and also provides order-of-magnitude quantitative agreement with previous investigations alike (Braginskii, 1958; Koshak et al., 2015; Plooster, 1971). All of these models (including ours) predict an initial rapid channel expansion rate, leveling off when the channel is cooling down. During the initial return stroke stage $(0.5-5~\mu s)$, our calculated radius is 8-42% smaller than the results obtained by Braginskii (1958) and Plooster (1971), shown in Table II of Plooster (1971). Koshak et al. (2015) improved on the channel radial expansion rate derived by Braginskii (1958) and found a good agreement with Plooster (1971) at the 35- μs mark. Both investigations yielded a 1.5-cm radius at 35 μs , while our simulations yielded a value 57% lower. Generally, the results are in good agreement with previous investigations. However, it should be noted that our peak channel expansion rate is ~ 500 m/s, which is a factor of 4 lower than in Koshak et al. (2015).

Figure 6e presents the resistance (per unit length) as a function of time. It can be seen that the resistance drops by more than two orders of magnitude while the current is rising, illustrating how negative differential resistance works for a current changing over time. After that, while the current is decreasing exponentially in time, the resistance achieves a stable value between $0.6-1~\Omega/m$. This leveling off is in agreement with the trend seen in measurements (Jayakumar et al., 2006, Figure 4). Jayakumar et al. (2006) measured the electrical current to ground and the vertical electric field in close vicinity to a series of rocket-triggered lightning strikes in Florida. At the instant of peak power, these authors found resistance values between 0.67 and $31~\Omega/m$ in eight different strikes. In our calculations, we obtain $R = 0.6~\Omega/m$, which is close to the lowest resistance value in their dataset. This value is closer to the measurements than the early estimate of $0.035~\Omega/m$ by Rakov (1998). Additionally, Jayakumar et al. (2006) registered input electrical energies between 0.9-6.4~kJ/m, also in range with our calculations.

Figure 6f shows the rates of electron-positive ion recombination. The figure shows a comparison between the rate of two- and three-body recombination with coefficients taken from Kossyi et al. (1992). The figure is included here to justify the model design assumptions discussed in section 2.2 (item #3). In the regime studied here and with the rate coefficients for an air plasma available in the literature, the three-body recombination rate is substantially slower than the two-body counterpart, justifying neglecting it in equation (3).

3.4. Behavior of Light Emission in Return Strokes

The net emission coefficient ϵ describes the radiative emission in all bands of the optical spectrum, encompassing the infrared, visible, and ultraviolet (Naghizadeh-Kashani et al., 2002). Most of the radiation escaping the plasma is in the vacuum ultraviolet range (wavelengths lower than 200 nm) and is caused by atomic emissions. However, this band is not easily detected because the radiation is readily absorbed by atmospheric-pressure air surrounding the plasma discharge (Cressault et al., 2015). Spectroscopic measurements of rocket-triggered lightning strikes show characteristic line emissions associated with neutral, singly, and doubly ionized nitrogen and oxygen, neutral argon, neutral hydrogen, and neutral copper (from the triggering wire) and present no detected molecular emissions (Walker & Christian, 2017).

For the purposes of comparing our simulations with observations, we estimate the power (per unit channel length) emitted in the *visible range* as $\eta_{\rm vis}4\pi\epsilon\pi r_{\rm c}^2$, where $\eta_{\rm vis}$ is the fraction of optical radiation emitted in the visible range (380–780 nm). We use a constant fraction $\eta_{\rm vis}=3\%$ for the sake of simplicity. In reality $\eta_{\rm vis}$ depends on the radial distribution of the plasma temperature and the cumulative balance of emission and absorption. Table 2 shows seven estimates of $\eta_{\rm vis}$ based on different references and techniques. Perhaps the most pertinent is estimate #2, which is calculated by taking the ratio of $\epsilon_{\rm vis}$ in the visible range calculated by Cressault et al. (2011, Figure 2) to ϵ in the total optical range calculated by (Naghizadeh-Kashani et al., 2002, Figure 13) for an optically thin plasma. This strategy places $\eta_{\rm vis}$ between 0.1% and 10% in the temperature range between 3,000 and 30,000 K. Within this range, we adopt the value of 3% because it yields a good agreement with experimental data from Quick and Krider (2017) discussed below.

Figure 7 shows properties of return stroke light emission and comparison to rocket-triggered lightning data collected by Quick & Krider (2017, Figures 15 and 16). From a 200-m distance to the lightning striking point, Quick and Krider (2017) recorded the luminosity of a 62-m-long channel segment near the ground. The radiometers used had an approximately flat spectral response in the 400- to 1,000-nm range. Figure 7a shows the simulated temporal dynamics of visible power and electrical current in the channel, for conditions that resemble the aforementioned observations. The waveform is $0.5/50 \,\mu s$ with a 12-kA peak current, similar to

Tab	· ·				
Fraction of Optical Power Radiated in the Visible Range by an Air Plasma					
#	Estimation method and reference	$\eta_{\mathrm{vis}}\left(\%\right)$			
1	Black-body spectral radiance (Siegel, 2001, p. 22) (3,000-30,000 K)	5.3-49			
2	Visible $\epsilon_{ m vis}$ calculated by Cressault et al. (2011) (3,000–30,000 K)	0.1-10			
3	Visible radiance calculated by Cressault et al. (2015) (8,000–30,000 K)	0.2-0.6			
4	20-kJ/m hot air shock (Ripoll et al., 2014a, Figure 9 and section 3.1)	14.3			
5	Several simulations in Table 1 of Ripoll et al. (2014a)	4-30			
6	Section 4.2 of Ripoll et al. (2014a)	5.3-21.7			
7	A 12-kA discharge (Ripoll et al., 2014b, Figures 9b and 10b)	30			
	Empirical (this work)	3			

the median case in the data set (Quick & Krider, 2017, Table 1). Figure 7b shows the first 3 μ s of light emission, evidencing a 0.1- μ s delay between the rise of current and optical emissions in the channel. Figure 7c shows the effects of increasing peak current, which lead to higher emitted power and longer duration of the light emission.

The delay shown in Figure 7b is evaluated at the 20% of peak level. The 0.1- μ s value is in excellent agreement with experimental results by Carvalho et al. (2014, 2015) and Quick and Krider (2017) who found delays of

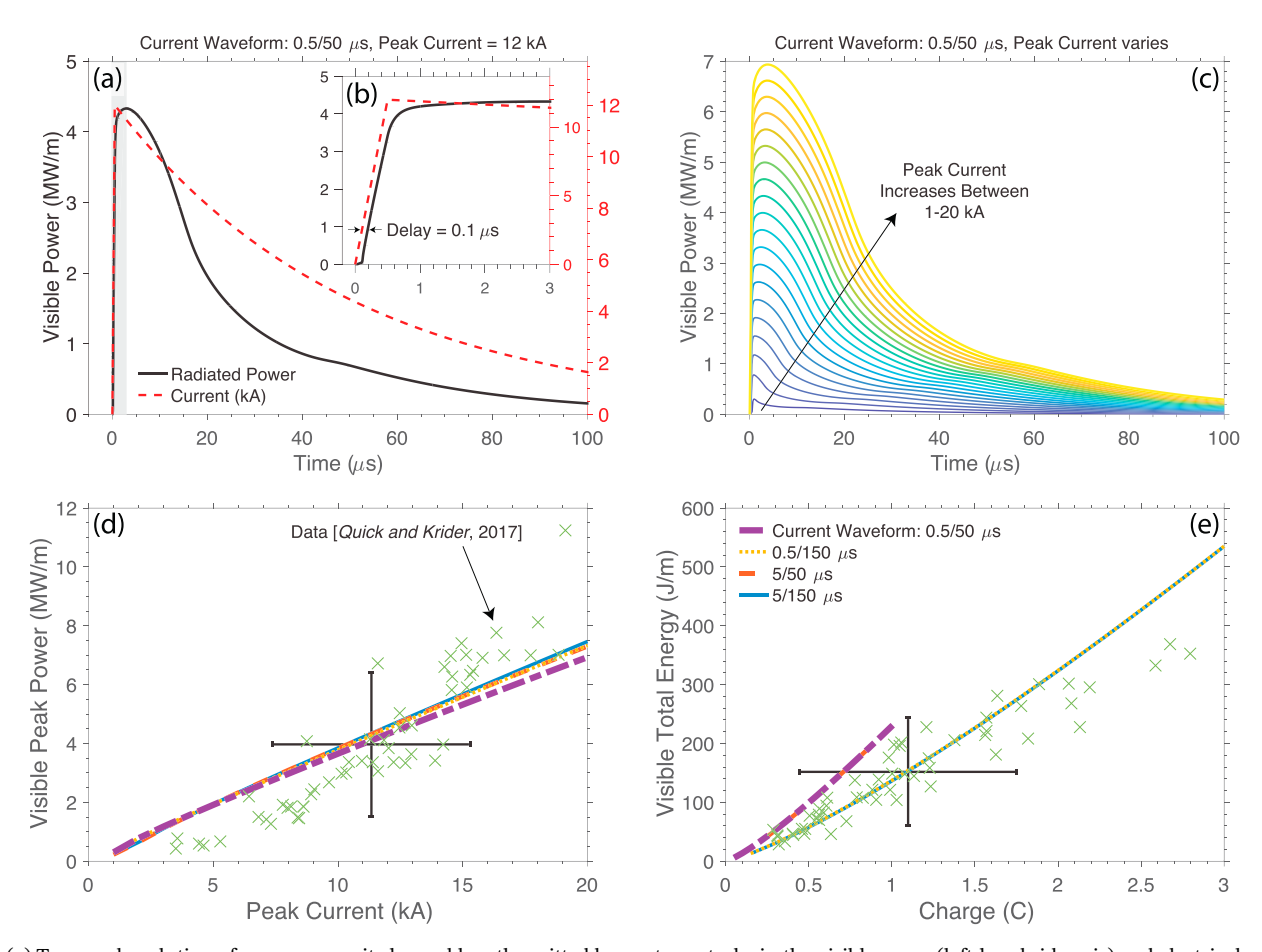


Figure 7. (a) Temporal evolution of power per unit channel length emitted by a return stroke in the visible range (left-hand side axis) and electrical current (right-hand side). Panel (b) is a zoom-in into the gray shaded rectangle in panel (a). (c) Visible power emitted for several different peak current values. (d) Visible peak power versus peak current for four different current waveforms. (e) Energy emitted in the visible range versus charge transferred to the ground (the integration time is 2 ms). Panels (d) and (e) show a comparison with the experimental data from Quick and Krider (2017). The big crosses indicate the average ± standard deviation in the dataset. The data were collected during a study conducted by the University of Arizona at the International Center for Lightning Research and Testing, in Camp Blanding, FL, in 2012.



 0.09 ± 0.05 and 0.09 ± 0.06 µs, respectively. Differently than Quick and Krider (2017), Carvalho et al. (2014) recorded luminosity from a 3-m-long channel segment near the ground. From such a short segment, the luminosity rise time is not masked by the geometrical growth of the return stroke in the field of view. The fact that both experimental investigations observing different channel lengths (62 and 3 m) yielded similar results lends robustness to the \sim 0.1 µs measured delay. Furthermore, analysis of different types of pulses occurring in the return stroke channel (Zhou et al., 2014) and of several channel segments at different heights (Carvalho et al., 2015) have led to the general conclusion that current and luminosity have similar rise times and the delay between the two has the same order of magnitude as such time scales. More precisely, Carvalho et al. (2015) found that the delay is approximately linearly dependent on the current rise time according to the following fit formula: delay = 0.35 $\tau_{\rm rise}^{1.03}$, where $\tau_{\rm rise}$ is the 10–90% current rise time given in microseconds. The fit comprises rise times between \sim 0.1 µs (for return strokes) and \sim 100 µs (for M components). Using this formula, we obtain a delay of 0.14 µs for the simulation shown in Figure 7b, once more indicating good agreement between simulation and measurements.

In our simulations the delay between the rise of current and optical emissions highlighted in Figure 7b has a clear interpretation. It is attributed to the finite time scale of channel heating and expansion. Since the initial channel temperature for the simulations shown in this section is 5000 K, non-LTE effects play a minor role here. From equations (1) and (2), the air heating rate thus is $\partial T/\partial t \simeq (I^2/\sigma_{\rm LTE}\pi^2r_c^2-4\pi\epsilon)/\rho_m c_p$. What determines the finite 0.1-µs delay, in a return stroke with 0.5-µs rise time, are the coefficients ρ_m , c_p , $\sigma_{\rm LTE}$, and ϵ , as well as the channel expansion $r_c(t)$. A comparison with a full-LTE version of the simulation code yielded a similar time delay between current and optical emissions, but the full-LTE model overestimated the peak optical power by a factor of 3–4.

Figures 7d and 7e show the peak visible power versus peak current and total energy versus charge, respectively. The integration time for the charge and energy is 2 ms. The figures show simulations for different current waveforms and comparison with light emitted by rocket-triggered lightning. The data correspond to optical irradiance from 55 rocket-triggered lightning strikes (with currents and charges ranging between 3–20 kA and 0.3–3 C, respectively) observed in Florida by Quick and Krider (2017) in 2012. The irradiance data is converted to power per unit channel length according to equation (2) in the original reference. The simulations use the same initial conditions as in Figure 6, and the results indicate a direct relationship between current and power and between total energy and charge. Additionally, the calculations (under the $\eta_{\rm vis}=3\%$ assumption) present good agreement with the observational data, especially near the average values (the big crosses in the figures). The peak visible power shows little dependence on the current waveform parameters in the range used ($\tau_{\rm r}=0.5$ and 5 $\mu{\rm s}$, and $\tau_{\rm f}=50$ and 150 $\mu{\rm s}$). The rise time also does not affect the relationship between energy emitted and charge transferred to the ground, shown in Figure 7e. The same figure also shows that strokes with a narrower current pulse (i.e., with shorter fall time) are more efficient in converting electrical energy into optical.

There are two important issues that must be noted about the comparison made in Figures 7d and 7e. First, the radiometers used by Quick and Krider (2017) have a flat spectral response in the 400-1,000 nm range. According to Ripoll et al. (2014a, 2014b), about twice as much energy is emitted in this range than in the visible, because it includes part of the infrared spectrum. Second, Quick and Krider (2017) state that rocket-triggered lightning strikes radiate around half as much energy as first strikes in natural cloud-to-ground flashes. But the simulations use initial conditions that best resemble first strikes in natural lightning, similarly to the works by Plooster (1971) and Paxton et al. (1986). Therefore, if we attempt to scale the numerical results to correspond to optical power emitted in the 400-1,000 nm range (\times 2) by rocket-triggered lightning (\times 1/2), the factors of two cancel and the curves would stay in the same place in Figures 7d and 7e, which lends further credence to the comparison. Nonetheless, it should be noted that our numerical investigations did not capture the approximate quadratic scaling between peak luminosity and peak current, that is, luminosity \times I_p^2 , seen in observations (Carvalho et al., 2015; Quick & Krider, 2017; Zhou et al., 2014). Further work is required to explain all experimentally inferred relationships between current and luminosity derived from close-by observations of rocket-triggered lightning.

When analyzing the light emission of return strokes, two additional factors must be noted. First, in rocket-triggered lightning there is a nonnegligible amount of copper emission within the visible spectrum,



arising from the vaporization of the copper wire that connects the rocket to the ground (Walker & Christian, 2017). Second, there is a geometric growth effect of the optical emission within the field of view of the detector. For the sake of simplicity, these two effects are neglected in the simulations by assuming that the fraction of total energy radiated by neutral copper is small in comparison to all other emissions from the air plasma, and by assuming that within the narrow field of view of the detector (only 62 m of channel length) the return stroke current amplitude does not change considerably. All these uncertainties are encapsulated within the parameter $\eta_{\rm vis}$, adjusted within reason to fit the measurements.

In all simulations shown in Figure 7, the total energy deposited in the channel by Joule heating ranges between 10 J/m and 18 kJ/m. At the instant of peak electrical power, the channel resistance varies between 0.6–130 Ω /m within all simulation cases presented in this section. For peak currents larger than 5 kA, this quantity shows little dependence on the current rise time and fall time values used, and can be fitted by the following formula $R = A/I_p$, where A = 13 kA Ω /m (the mean error between fit and simulation results is lower than 3%). From this formula it is easy to see that in the range of peak currents between 10 and 20 kA, the channel resistance per unit length at the instant of peak electrical power reduces from 1.3 to 0.65 Ω /m. Once again these values are in good agreement with the experimental findings of Jayakumar et al. (2006, Table 2).

4. Summary and Conclusions

In summary, in this manuscript we introduced, validated, and used a physics-based computational tool to calculate the lightning channel's nonlinear plasma resistance. A model that bridges an existing gap in the literature, by providing a self-consistent evaluation of the plasma properties at little computational cost (i.e., at the cost of solving five ordinary differential equations). In this paper, we showed how the proposed computer-simulation tool can perform well in a wide range of current values, from 1 to 10⁴ A. It can capture well the non-LTE plasma regime, by reproducing the finite time scale for streamer-to-leader transition with reasonable accuracy. Furthermore, in the high-current/full-LTE regime, the model can capture well the temporal evolution of the neutral-gas temperature and the estimated energy deposition by a return stroke, in good agreement with the work of Plooster (1971) and Paxton et al. (1986).

The model also describes well the negative differential resistance behavior of steady-state arc discharges, in good agreement with the experimental findings of King (1961) and Tanaka et al. (2000). The steady-state resistance in the millisecond time scale has an inverse power law dependence on the current, that is, $R = A/I^b$, where A and b are fitting constants. We found that the power law index b decreases with increasing current, because at different current regimes the steady state is dictated by distinct physical processes. At low currents (I < 10 A) the steady state is given by a balance of Joule heating and heat conduction, while at high currents (I > 1 kA) the steady state is given by a balance with radiative losses. The intermediate current range is marked by a comparable role between the two loss processes, with radiative emission being important in the submillisecond time scale, while heat conduction being significant at later stages.

We presented a detailed description of the light emission in a return stroke. We showed that the proposed model can reproduce the experimentally inferred direct relationship between peak current and peak radiated power and between charge transferred to ground and total energy radiated, as experimentally inferred by Quick and Krider (2017). The caveat is that the quadratic power law relationship between the two remains unexplained. The model also captures the 0.1- μs delay between the rise of current and optical emissions in rocket-triggered lightning return strokes, as measured with high precision by Carvalho et al. (2014, 2015).

It has been suggested that the negative differential resistance behavior of lightning channels plays an important role in the mechanism of current cutoff, which in its turn makes some flashes transfer charge to ground by a series of (discrete) return strokes, while others by a single stroke followed by a long continuing current (Krehbiel et al., 1979; Hare et al., 2019; Heckman, 1992; Mazur et al., 1995). Recent review articles argue that the role of negative differential resistance in the channel cutoff remains to be quantified (Mazur & Ruhnke, 2014; Williams, 2006; Williams & Heckman, 2012; Williams & Montanyà, 2019). The model described in this manuscript can be applied for simulating multiple return strokes in a flash and other types of processes taking place in the lightning channel, such as dart-leader ionization waves and M components, provided that the current waveform is given (see Figure 1b). Suggestions of future work include coupling this tool to



distributed circuit models of the lightning return stroke, or to fractal models of the growing lightning-leader network. We speculate that this strategy will provide important insights into the physics of lightning channel cutoff.

Acknowledgments

This research was supported by a Research Infrastructure Development award from New Mexico NASA EPSCoR. We have made the simulation data output (da Silva, 2019b) and rate coefficients (da Silva, 2019a) shown in this manuscript publicly available online.

References

- Aleksandrov, N. L., Bazelyan, E. M., Kochetov, I. V., & Dyatko, N. A. (1997). The ionization kinetics and electric field in the leader channel in long air gaps. *Journal of Physics D: Applied Physics*, 30, 1616–1624. https://doi.org/10.1088/0022-3727/30/11/011
- Aleksandrov, N. L., Bazelyan, E. M., & Konchakov, A. M. (2001). Plasma parameters in the channel of a long leader in air. *Plasma Physics Reports*, 27, 875–885. https://doi.org/10.1134/1.1409721
- Aleksandrov, N. L., Bazelyan, E. M., & Shneider, M. N. (2000). Effect of continuous current during pauses between successive strokes on the decay of the lightning channel. *Plasma Physics Reports*, 26(10), 893–901. https://doi.org/10.1134/1.1316830
- Baker, L. (1990). Return-stroke transmission line model. In R. L. Gardner (Ed.), *Lightning electromagnetics* (pp. 63–74). Philadelphia, PA: Taylor and Francis.
- Barannik, S. I., Vasserman, S. B., & Lukin, A. N. (1975). Resistance and inductance of a gas arc. Soviet physics. Technical physics, 19(11), 1499–1453.
- Bazelyan, E. M., & Raizer, Y. P. (1998). Spark discharge. Boca Raton/Florida: CRC Press.
- Bazelyan, E. M., & Raizer, Y. P. (2000). Lightning physics and lightning protection. Bristol/Philadelphia: Institute of Physics Publishing.
- Bazelyan, E. M., Raizer, Y. P., & Aleksandrov, N. L. (2007). The effect of reduced air density on streamer-to-leader transition and on properties of long positive leader. *Journal of Physics D: Applied Physics*, 40(14), 4133–4144. https://doi.org/10.1088/0022-3727/40/14/007
- Becker, K. H., Kogelschatz, U., Schoenbach, K. H., & Barker, R. J. (2004). Non-equilibrium air plasmas at atmospheric pressure (pp. 700). Boca Raton, FL: CRC Press. https://doi.org/10.1201/9781482269123
- Benilov, M. S., & Naidis, G. V. (2003). Modelling of low-current discharges in atmospheric-pressure air taking account of non-equilibrium effects. *Journal of Physics D: Applied Physics*, 36, 1834–1841. https://doi.org/10.1088/0022-3727/36/15/314
- Bittencourt, J. A. (2004). Fundamentals of plasma physics (3rd ed.). New York: Springer.
- Boulos, M. I., Fauchais, P., & Pfender, E. (1994). Thermal plasmas, fundamentals and applications (Vol. 1). New York: Plenum.
- Braginskii, S. I. (1958). Theory of the development of a spark channel. Soviet Physics-JETP, 34(6), 1068-1074.
- Bruce, C. E. R., & Golde, R. H. (1941). The lightning discharge. Journal of the Institution of Electrical Engineers—Part II: Power Engineering, 88(6), 487–505. https://doi.org/10.1049/ji-2.1941.0065
- Carvalho, F. L., Jordan, D. M., Uman, M. A., Ngin, T., Gamerota, W. R., & Pilkey, J. T. (2014). Simultaneously measured lightning return stroke channel-base current and luminosity. *Geophysical Research Letters*, 41, 7799–7805. https://doi.org/10.1002/2014GL062190
- Carvalho, F. L., Uman, M. A., Jordan, D. M., & Ngin, T. (2015). Lightning current and luminosity at and above channel bottom for return strokes and M-components. *Journal Geophysical Research: Atmospheres*, 120, 10,645–10,663. https://doi.org/10.1002/2015JD023814
- Černák, M., van Veldhuizen, E. M., Morva, I., & Rutgers, W. R. (1995). Effect of cathode surface properties on glow-to-arc transition in a short positive corona gap in ambient air. *Journal of Physics D: Applied Physics*, 28, 1126–1132. https://doi.org/10.1088/0022-3727/28/6/
- Chemartin, L., Lalande, P., Montreuil, E., Delalondre, C., Cheron, B. G., & Lago, F. (2009). Three dimensional simulation of a DC free burning arc. Application to lightning physics. *Atmospheric Research*, 91(2-4), 371–380. https://doi.org/10.1016/j.atmosres.2008.07.009
- Cho, M., & Rycroft, M. J. (1998). Computer simulation of the electric field structure and optical emission from cloud-top to the ionosphere. Journal of Atmospheric and Solar-Terrestrial Physics, 60(7-9), 871–888. https://doi.org/10.1016/S1364-6826(98)00017-0
- Cressault, Y., Bauchire, J. M., Hong, D., Rabat, H., Riquel, G., Sanchez, F., & Gleizes, A. (2015). Radiation of long and high power arcs. Journal of Physics D: Applied Physics, 48(41), 415201. https://doi.org/10.1088/0022-3727/48/41/415201
- Cressault, Y., Gleizes, A., & Riquel, G. (2011). Calculation of the radiation emitted by isothermal arc plasmas in air and air-metal mixtures. In XX International Symposium on Plasma Chemistry (ISPC), Philadelphia, USA.
- da Silva, C. L. (2015). Numerical modeling of leader discharge mechanisms in lightning, blue jets, gigantic jets, and sprites (Ph.D. thesis), Penn State University University Park, PA.
- da Silva, C. L. (2019a). Rate coefficients used in the plasma nature of lightning channels and the resulting nonlinear resistance. Zenodo, Software https://doi.org/10.5281/zenodo.2597562
- da Silva, C. L. (2019b). Simulation data output used in the plasma nature of lightning channels and the resulting nonlinear resistance. Zenodo, Dataset https://doi.org/10.5281/zenodo.2597552
- da Silva, C. L., Merrill, R. A., & Pasko, V. P. (2016). Mathematical constraints on the use of transmission line models to investigate the preliminary breakdown stage of lightning flashes. *Radio Science*, 51, 367–380. https://doi.org/10.1002/2015RS005853
- da Silva, C. L., & Pasko, V. P. (2012). Simulation of leader speeds at gigantic jet altitudes. *Geophysical Research Letters*, 39, L13805. https://doi.org/10.1029/2012GL052251
- da Silva, C. L., & Pasko, V. P. (2013). Dynamics of streamer-to-leader transition at reduced air densities and its implications for propagation of lightning leaders and gigantic jets. *Journal of Geophysical Research: Atmospheres*, 118, 13,561–13,590. https://doi.org/10.1002/2013JD020618
- da Silva, C. L., & Pasko, V. P. (2014). Infrasonic acoustic waves generated by fast air heating in sprite cores. *Geophysical Research Letters*, 41, 1789–1795. https://doi.org/10.1002/2013GL059164
- De Conti, A., Visacro, S., Theethayi, N., & Cooray, V. (2008). A comparison of different approaches to simulate a nonlinear channel resistance in lightning return stroke models. *Journal of Geophysical Research*, 113, D14129. https://doi.org/10.1029/2007JD009395
- Engel, T. G., Donaldson, A. L., & Kristiansen, M. (1989). The pulsed discharge arc resistance and its functional behavior. IEEE Transactions on Plasma Science, 17(2), 323–329. https://doi.org/10.1109/27.24643
- Flitti, A., & Pancheshnyi, S. (2009). Gas heating in fast pulsed discharges in N₂–O₂ mixtures. *The European Physical Journal Applied Physics*, 45(2), 21001. https://doi.org/10.1051/epjap/2009011
- Gallimberti, I. (1979). The mechanism of the long spark formation. Journal de Physique Colloques, 40(C7), 193-250.
- Gallimberti, I., Bacchiega, G., Bondiou-Clergerie, A., & Lalande, P. (2002). Fundamental processes in long air gap discharges. *Comptes Rendus Physique*, 3, 1335–1359. https://doi.org/10.1016/S1631-0705(02)01414-7
- Hare, B. M., Scholten, O., Dwyer, J., Trinh, T. N. G., Buitink, S., ter Veen, S., et al. (2019). Needle-like structures discovered on positively charged lightning branches. *Nature*, 568(7752), 360–363. https://doi.org/10.1038/s41586-019-1086-6
- Heckman, S. (1992). Why does a lightning flash have multiple strokes? (Ph.D. thesis), Massachusetts Institute of Technology, Cambridge.



- Heidler, F. (1985). Traveling current source model for LEMP calculation, *Proc. 6th Int. Zurich Symp. Electromagnetic Compatibility* (pp. 157–162). Switzerland: Zurich.
- Hill, R. . D. (1971). Channel heating in return-stroke lightning. *Journal of Geophysical Research*, 76(3), 637–645. https://doi.org/10.1029/JC076i003p00637
- Jayakumar, V., Rakov, V. A., Miki, M., Uman, M. A., Schnetzer, G. H., & Rambo, K. J. (2006). Estimation of input energy in rocket-triggered lightning. Geophysical Research Letters, 33, L05702. https://doi.org/10.1029/2005GL025141
- King, L. A. (1961). The voltage gradient of the free-burning arc in air or nitrogen. British Electrical and Allied Industries Research Association, Reference G/XT172.
- Koshak, W. J., Solakiewicz, R. J., & Peterson, H. S. (2015). A return stroke NO_X production model. *Journal of the Atmospheric Sciences*, 72(2), 943–954. https://doi.org/10.1175/JAS-D-14-0121.1
- Kossyi, I. A., Kostinsky, A. Y., Matveyev, A. A., & Silakov, V. P. (1992). Kinetic scheme of the non-equilibrium discharge in nitrogen-oxygen mixtures. *Plasma Sources Science and Technology*, 1, 207–220. https://doi.org/10.1088/0963-0252/1/3/011
- Krehbiel, P. R., Brook, M., & McCrory, R. A. (1979). An analysis of the charge structure of lightning discharges to ground. *Journal of Geophysical Research*, 84(C5), 2432–2456. https://doi.org/10.1029/JC084iC05p02432
- Kushner, M. J., Kimura, W. D., & Byron, S. R. (1985). Arc resistance of laser-triggered spark gaps. *Journal of Applied Physics*, 58(5), 1744–1751. https://doi.org/10.1063/1.336023
- Larsson, A. (1998). The effect of a large series resistance on the streamer-to-spark transition in dry air. *Journal of Physics D: Applied Physics*, 31, 1100–1108. https://doi.org/10.1088/0022-3727/31/9/011
- Liang, C., Carlson, B., Lehtinen, N., Cohen, M., Marshall, R. A., & Inan, U. S. (2014). Differing current and optical return stroke speeds in lightning. *Geophysical Research Letters*, 41, 2561–2567. https://doi.org/10.1002/2014GL059703
- Liu, N. Y., & Pasko, V. P. (2004). Effects of photoionization on propagation and branching of positive and negative streamers in sprites. Journal of Geophysical Research, 109, A04301. https://doi.org/10.1029/2003JA010064
- Lowke, J. J., Kovitya, P., & Schmidt, H. P. (1992). Theory of free-burning arc columns including the influence of the cathode. *Journal of Physics D: Applied Physics*, 25(11), 1600–1606. https://doi.org/10.1088/0022-3727/25/11/006
- Luque, A., & Gordillo-Vázquez, F. J. (2012). Mesospheric electric breakdown and delayed sprite ignition caused by electron detachment. Nature Geoscience, 5(1), 22–25. https://doi.org/10.1038/NGEO1314
- Marode, E., Bastien, F., & Bakker, M. (1979). A model of the streamer-induced spark formation based on neutral dynamics. *Journal of Applied Physics*, 50, 140–146. https://doi.org/10.1063/1.325697
- Mattos, M. A. F., & Christopoulos, C. (1990). A model of the lightning channel, including corona, and prediction of the generated
- electromagnetic fields. Journal of Physics D: Applied Physics, 23(1), 40. https://doi.org/10.1088/0022-3727/23/1/007 Mazur, V., Krehbiel, P. R., & Shao, X.-M. (1995). Correlated high-speed video and radio interferometric observations of a cloud-to-ground
- lightning flash. Journal Geophysical Research, 100(D12), 25,731–25,753. https://doi.org/10.1029/95JD02364 Mazur, V., & Ruhnke, L. H. (2014). The physical processes of current cutoff in lightning leaders. Journal Geophysical Research: Atmospheres,
- 119, 2796–2810. https://doi.org/10.1002/2013JD020494 Montano, R., Becerra, M., Cooray, V., Rahman, M., & Liyanage, P. (2006). Resistance of spark channels. *IEEE Transactions on Plasma*
- Science, 34(5), 1610–1619. https://doi.org/10.1109/TPS.2006.883350

 Morrow, R., & Lowke, J. J. (1997). Streamer propagation in air. Journal of Physics D: Applied Physics, 30, 614–627. https://doi.org/10.1088/
- 0022-3727/30/4/017 Naghizadeh-Kashani, Y., Cressault, Y., & Gleizes, A. (2002). Net emission coefficient of air thermal plasmas. *Journal of Physics D: Applied*
- Physics, 35(22), 2925. https://doi.org/10.1088/0022-3727/35/22/306
 Naidis, G. (1999). Simulation of streamer-to-spark transition in short non-uniform air gaps. Journal of Physics D: Applied Physics, 32(20), 2649–2654. https://doi.org/10.1088/0022-3727/32/20/311
- Naidis, G. V. (2005). Dynamics of streamer breakdown of short non-uniform air gaps. Journal of Physics D: Applied Physics, 38(21), 3889–3893. https://doi.org/10.1088/0022-3727/38/21/009
- Naidis, G. V. (2009). Positive and negative streamers in air: Velocity-diameter relation. *Physical Review E*, 79(5), 57401. https://doi.org/10. 1103/PhysRevE.79.057401
- Pancheshnyi, S., Nudnova, M., & Starikovskii, A. (2005). Development of a cathode-directed streamer discharge in air at different pressures: Experiment and comparison with direct numerical simulation. *Physical Review E*, 71, 16407. https://doi.org/10.1103/PhysRevE.71.016407
- Paxton, A. H., Gardner, R. L., & Baker, L. (1986). Lightning return stroke. A numerical calculation of the optical radiation. *Physics Fluids*, 29(8), 2736–2741. https://doi.org/10.1063/1.865514
- Plooster, M. N. (1971). Numerical model of the return stroke stroke of the lightning discharge. *Physics Fluids*, 14(10), 2124–2133. https://doi.org/10.1063/1.1693303
- Popov, N. A. (2001). Investigation of the mechanism for rapid heating of nitrogen and air in gas discharges. *Plasma Physics Reports*, 27(10), 886–896. https://doi.org/10.1134/1.1409722
- Popov, N. A. (2003). Formation and development of a leader channel in air. Plasma Physics Reports, 29(8), 695–708. https://doi.org/10. 1134/1.1601648
- Popov, N. A. (2009). Study of the formation and propagation of a leader channel in air. *Plasma Physics Reports*, 35, 785–793. https://doi.org/10.1134/S1063780X09090074
- Popov, N. A. (2011). Fast gas heating in a nitrogen-oxygen discharge plasma: I. Kinetic mechanism. *Journal of Physics D: Applied Physics*, 44, 285201. https://doi.org/10.1088/0022-3727/44/28/285201
- Quick, M. G., & Krider, P. E. (2017). Optical power and energy radiated by return strokes in rocket-triggered lightning. *Journal Geophysics Research: Atmospheres*, 122, 8816–8832. https://doi.org/10.1002/2017JD027363
- Raizer, Y. P. (1991). Gas discharge physics. New York: Springer-Verlag.
- Rakov, V. A. (1998). Some inferences on the propagation mechanisms of dart leaders and return strokes. *Journal Geophysics Research*, 103(D2), 1879–1887. https://doi.org/10.1029/97JD03116
- Rakov, V. A., & Uman, M. A. (1998). Review and evaluation of lightning return stroke models including some aspects of their application. *IEEE Transactions on Electromagnetic Compatibility*, 40(4), 403–426. https://doi.org/10.1109/15.736202
- Rakov, V. A., & Uman, M. A. (2003). Lightning: Physics and effects (pp. 687). Cambridge: University Press.
- Rayment, S. W., & Moruzzi, J. L. (1978). Electron detachment studies between O⁻ ions and nitrogen. *International Journal of Mass Spectrometry and Ion Processes*, 26(3), 321–326. https://doi.org/10.1016/0020-7381(78)80033-3
- Riousset, J. A., Pasko, V. P., & Bourdon, A. (2010). Air-density-dependent model for analysis of air heating associated with streamers, leaders, and transient luminous events. *Journal Geophysical Research*, 115, A12321. https://doi.org/10.1029/2010JA015918



- Ripoll, J.-F., Zinn, J., Colestock, P. L., & Jeffery, C. A. (2014b). On the dynamics of hot air plasmas related to lightning discharges: 2. Electrodynamics. *Journal Geophysical Research: Atmospheres*, 119, 9218–9235. https://doi.org/10.1002/2013JD020068
- Ripoll, J.-F., Zinn, J., Jeffery, C. A., & Colestock, P. L. (2014a). On the dynamics of hot air plasmas related to lightning discharges: 1. Gas dynamics. *Journal Geophysical Research: Atmospheres*, 119, 9196–9217. https://doi.org/10.1002/2013JD020067
- Sansonnens, L., Haidar, J., & Lowke, J. J. (2000). Prediction of properties of free burning arcs including effects of ambipolar diffusion. Journal of Physics D: Applied Physics, 33(2), 148. https://doi.org/10.1088/0022-3727/33/2/309
- Siegel, R. (2001). Thermal radiation heat transfer (4th ed., Vol. 1, pp. 864). New York: CRC Press.
- Takaki, K., & Akiyama, H. (2001). The resistance of a high-current pulsed discharge in nitrogen. *Japanese Journal of Applied Physics*, 40(Part 1, No. 2B), 979–983. https://doi.org/10.1143/jjap.40.979
- Tanaka, S., Sunabe, K., & Goda, Y. (2000). Three dimensional behaviour analysis of D.C. free arc column by image processing technique. In XIII Int'l. Conf. on Gas Discharges and Their Applications, Glasgow.
- Tanaka, M., Terasaki, H., Ushio, M., & Lowke, J. J. (2003). Numerical study of a free-burning argon arc with anode melting. *Plasma Chemistry and Plasma Processing*, 23(3), 585–606. https://doi.org/10.1023/A:1023272007864
- Theethayi, N., & Cooray, V. (2005). On the representation of the lightning return stroke process as a current pulse propagating along a transmission line. *IEEE Transactions on Power Delivery*, 20(2), 823–837. https://doi.org/10.1109/TPWRD.2004.839188
- Vidal, F., Gallimberti, I., Rizk, F. A. M., Johnston, T. W., Bondiou-Clergerie, A., Comtois, D., et al. (2002). Modeling of the air plasma near the tip of the positive leader. *IEEE Transactions on Plasma Science*, 30(3), 1339–1349. https://doi.org/10.1009/TPS.2002.801538
- Walker, T. D., & Christian, H. J. (2017). Triggered lightning spectroscopy: Part 1. A qualitative analysis. Journal of Geophysical Research: Atmospheres. 122, 8000–8011. https://doi.org/10.1002/2016JD026419
- Walker, T. D., & Christian, H. J. (2019). Triggered lightning spectroscopy: 2. A quantitative analysis. *Journal of Geophysical Research:* Atmospheres, 124, 3930–3942. https://doi.org/10.1029/2018JD029901
- Williams, E. R. (2006). Problems in lightning physics—The role of polarity asymmetry. *Plasma Sources Science and Technology*, 15, S91—S108. https://doi.org/10.1088/0963-0252/15/2/S12
- Williams, E. R., & Heckman, S. (2012). Polarity asymmetry in lightning leaders: The evolution of ideas on lightning behavior from strikes to aircraft. *Journal Aerospace Lab*, 5, AL05–04.
- Williams, E., & Montanyà, J. (2019). A closer look at lightning reveals needle-like structures. *Nature*, 568, 319–320. https://doi.org/10.1038/d41586-019-01178-7
- Winn, W. P., Aulich, G. D., Hunyady, S. J., Eack, K. B., Edens, H., Krehbiel, P. R., et al. (2011). Lightning leader stepping, K changes, and other observations near an intracloud flash. *Journal Geophysical Research*, 116, D23115. https://doi.org/10.1029/2011JD015998
- Yos, J. M. (1963). Transport properties of nitrogen, hydrogen, oxygen, and air to 30,000° K (Tech. Rep.) Wilmington, MA: AVCO Corp. Tech. Memo. RAD-TM-63-7.
- Zhou, M., Wang, D., Wang, J., Takagi, N., Gamerota, W. R., Uman, M. A., et al. (2014). Correlation between the channel-bottom light intensity and channel-base current of a rocket-triggered lightning flash. *Journal Geophysical Research: Atmospheres*, 119, 13,457–13,473. https://doi.org/10.1002/2014JD022367